Drag De-Orbit Device (D3): A Retractable Device for CubeSat Attitude and Orbit Control using Aerodynamic Forces

David Guglielmo[a], Sanny Omar[b], and Riccardo Bevilacqua[c]
University of Florida, 939 Sweet Water Drive, Gainesville, FL, 32611

The increasing number of CubeSats being launched has raised concerns about orbital debris since most of these satellites have no means of active orbit control. Some technologies exist to increase the surface area of a CubeSat and expedite de-orbit due to aerodynamic drag in low Earth orbit, but most of these devices cannot be retracted and hence cannot be used for orbital maneuvering. This paper discusses the De-Orbit Drag Device (D3) module that is capable of de-orbiting a 12U, 15kg CubeSat from a 700 km circular orbit in under 25 years and can be deployed and retracted to modulate the aerodynamic drag force experienced by the satellite. This facilitates orbital maneuvering using aerodynamic drag and the active targeting of a de-orbit location. In addition, the geometry of this drag device provides 3-axis attitude stabilization of the host CubeSat using aerodynamic and gravity gradient torques which is useful for many missions and provides a predictable aerodynamic profile for use in orbital maneuvering algorithms.

[a] Post-Doctoral Research Assistant, Mechanical and Aerospace Engineering Department, MAE-A 211, and AIAA Member.

[b] Graduate Research Assistant, Mechanical and Aerospace Engineering Department, MAE-A 211, and AIAA Student Member.

[c] Associate Professor, Mechanical and Aerospace Engineering Department, MAE-A 308, and AIAA Senior Member.

Nomenclature

a	=	Semi-major axis (km)
$\vec{a}$	=	Semi-major axis vector (km)
A	=	Cross sectional area $\left(m^2\right)$
a_d	=	Drag acceleration $\left(\frac{km}{s}\right)$
ADACS	=	Attitude Determination And Control System
B	=	Magnetic flux density (T)
B_r	=	Magnetic remanance (T)
B_s	=	Magnetic saturation (T)
B_{Earth}	=	Earth's magnetic field (T)
$\dot{B}$	=	Rate of change of Earth's measured magnetic field $\left(\frac{T}{sec}\right)$
C_b	=	Ballistic coefficient
C_d	=	Drag coefficient
COTS	=	Commercial Off The Shelf
e	=	Eccentricity
ECI	=	Earth-Centered Inertial
GTO	=	Geostationary Transfer Orbit
H	=	Magnetizing field $\left(\frac{A}{m}\right)$
H_c	=	Magnetic coercivity $\left(\frac{A}{m}\right)$
I	=	Current (A)
I	=	Area moment of inertia $\left(m^4\right)$
i	=	Orbital inclination (rad)
IR	=	Infrared
ISS	=	International Space Station
J_2	=	Second order harmonic of Earth gravitational potential field (Earth flattening)
LEO	=	Low Earth Orbit
m	=	Spacecraft mass (kg)
$\vec{M}$	=	Spacecraft magnetic dipole moment $\left(\frac{J}{T}\right)$
n	=	Number of turns
NASA	=	National Aeronautics and Space Administration
NED	=	North East Down Frame
Q	=	Heat transfer rate $\left(\frac{J}{sec}\right)$

r	=	ECI position (km)
$\vec{r}$	=	ECI position vector (km)
$\hat{s}$	=	Coil normal vector
SoC	=	System-on-a-Chip
SRP	=	Solar Radiation Pressure
T	=	Temperature (K)
t	=	Time (sec)
U	=	CubeSat Standardized Unit, $10cmx10cmx10cm$
USAF	=	United States Air Force
v_∞	=	Velocity through a medium $\left(\frac{km}{s}\right)$
$\vec{v}_\infty$	=	Velocity vector through a medium $\left(\frac{km}{s}\right)$
$alpha$	=	Angular acceleration vector $\left(\frac{rad}{s^2}\right)$
ΔV	=	Change in velocity required to perform an orbital maneuver $\left(\frac{km}{s}\right)$
ϵ	=	Emissivity
θ	=	True anomaly (rad)
μ	=	Magnetic torque $(N \cdot m)$
μ_0	=	Permeability of free space $\left(1.25663706 * 10^{-6} \frac{m \cdot kg}{s^2 \cdot A^2}\right)$
μ_E	=	Earth gravitational parameter $\left(3.98574405096 * 10^{14} \frac{m^3}{s^2}\right)$
ρ	=	Atmospheric density $\left(\frac{kg}{m^3}\right)$
σ	=	Stefan-Boltzmann Constant $\left(5.670367 \cdot 10^{-8} \frac{W}{m^2 \cdot K^4}\right)$ [1]
$\vec{\tau}$	=	Magnetic torque on spacecraft $(N \cdot m)$
Ω	=	Right Ascension of the Ascending Node (RAAN) (rad)
ω	=	Argument of periapsis (rad)

I. Introduction

As more and more spacecraft are launched, LEO (Low Earth Orbit) is becoming more crowded. Many small spacecraft launch as a secondary payloads and if they have no propulsions systems, are constrained to operating in the orbits of the primary payload. CubeSats, small spacecraft primarily designed for university and research use, are a common example. Popular orbits such as sun-synchronous and space station orbits have become particularly crowded due to the increasing number of CubeSats being deployed into these orbits as secondary payloads. Additionally, the

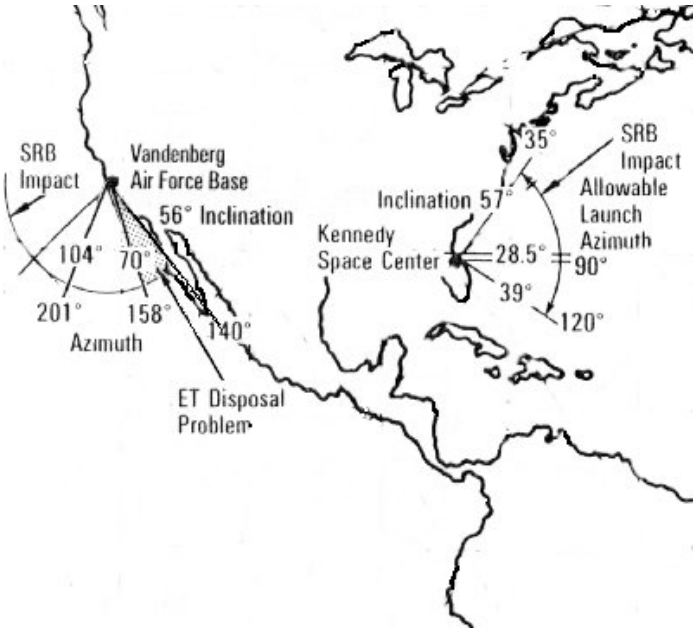

Fig. 1 Kennedy and Vandenberg Launch Inclinations (Image Courtesy NASA)

minimum inclination of an orbit, if no plane change maneuvers are used, is equal to the latitude of the launch site, since the orbital plane must pass through the center of the Earth [2]. Furthermore, In order to avoid upper stages or aborted missions falling on populated areas, each location must launch over the ocean, further restricting the possible inclinations. The Kennedy Space Center and Vandenburg Air Force Base launch sites utilized by NASA and the United States Air Force are shown in Figure 1 which details the possible launch inclinations from each location.

The increasing number of small spacecraft in popular low Earth orbits has led to stricter regulations on orbital debris mitigation and the desire for improved orbital maneuvering capabilities to avoid collisions between satellites. Different techniques have been proposed for relative maneuvering between spacecraft in LEO, for both collision avoidance and formation flight. To further reduce the chances of collision, small spacecraft are also required to de-orbit within 25 years, as per NASA-STD-8719.14A [3]. Spacecraft in high orbits can take hundreds of years to deorbit (depending on altitude), but spacecraft cannot remain operational indefinitely. After the operational lifetime of a spacecraft has elapsed, if it has not deorbited, it becomes uncontrolled space debris. A piece of space debris can collide with other space objects, creating even more debris in a process known as Kessler Syndrome [4].

Many de-orbit methods have been previously proposed. Spacecraft have traditionally been de-orbited with thrusters or drag in LEO, but techniques using SRP (Solar Radiation Pressure) [5] have also been developed. Using drag to de-orbit is a passive method, and can be expedited by the deployment of a large aerodynamic device. Various hardware configurations have been developed, such as the Terminator Tape™ [6] and Terminator Tether™ [7], Deorbit and Recovery System (DRS) [8], Gossamer Orbit Lowering Device (GOLD) [9], AEOLDOS [10], the iDOD [11], Deutsche Orbitale Servicing Mission (DEOS) [12], and drag sails [13]. Increasing the drag sufficiently will decrease the orbit lifetime of a LEO spacecraft, but the eventual landing location will be uncontrolled. NASA-STD-8719.14A mandates that any spacecraft utilizing controlled re-entry techniques must land 370 km away from land and that the probability of targeting failure multiplied by the chance of human casualty due to the uncontrolled re-entry be less than 1 in 10,000 [3]. Spacecraft containing thrusters can relatively easily perform an impulsive de-orbit burn to ensure that their debris lands away from populated areas as was the case with the Delta IV upper stages [14] and the Mir space station [15]. However, a failure of the propulsion system can result in uncontrolled re-entry and pose a significant hazard to persons or property on the ground such as when Skylab fell over Australia in 1979 and generated a debris field in the Australian Outback [16].

Differential drag techniques, or modifying the relative drag-induced acceleration between two spacecraft, have been proposed previously by Leonard in 1986 [17] as means of thruster-free orbital maneuvering, and then built upon by many researchers since then, including some of the authors [18–20]. By modulating the drag area of a spacecraft appropriately, the spacecraft can also be made to de-orbit away from populated areas without the use of any thrusters. This technique could be used to save fuel for spacecraft containing thrusters and could be used to provide controlled re-entry for spacecraft whose thrusters have failed or that do not contain thrusters. The variation of atmospheric drag can be performed in several different ways including a rotation of the spacecraft panels [21] or the deployment of a drag device [22, 23]. Some of the authors have previously developed a repeatedly-retractable drag sail that can be modulated to produce changes in the satellite drag area [23].

Regardless of the method used, some measure of attitude control is necessary to maintain

a predictable drag area for aerodynamically-based orbital maneuvering algorithms. Commercial-Off-The-Shelf (COTS) ADACS (Attitude Determination And Control System) such as the BCT (Blue Canyon Technologies) XACT [24], MAI-400 (Maryland Aerospace, Inc.) [25] and a unit by ClydeSpace [26] are available for small spacecraft but can easily cost tens of thousands of dollars in addition to requiring significant mass and power onboard the host satellite.

This paper discusses the development of a retractable drag device for small spacecraft capable of modulating the drag area while providing 3-axis attitude stabilization using passive aerodynamic and gravity gradient torques and active damping using magnetorquers [27]. This De-Orbit Drag Device (D3) can be utilized for orbital maneuvering, de-orbit point targeting for spacecraft containing components that may survive re-entry, and for passive, uncontrolled de-orbit for spacecraft that will disintegrate on re-entry. The system is unique in that it can provide simultaneous attitude stabilization and modulation of the spacecraft's drag area, a capability not shared by any commercially available drag devices. The simplicity and limited number of moving parts in the D3 system also make it a cheaper and more reliable alternative to conventional ADACS units for many satellite missions without strict pointing requirements. For example, a satellite needing to point an antenna and camera within 20 degrees of the nadir vector, maintain a desired separation between sister satellites in the same orbital plane, and de-orbit once its mission is complete could utilize the D3 exclusively as its attitude and orbit control system.

The D3 consists of four measuring-tape-style booms, each of which is 4cm wide, 3.7m long when fully deployed, and inclined at 20 degrees relative to the rear face of the satellite. The dart configuration of these booms causes the satellite to naturally ram-align due to aerodynamic forces. Partially retracting two of the booms opposite each other results in a clear minimum moment of inertia axis which will simultaneously tend to align with the nadir vector due to gravity gradient torques, resulting in 3-axis attitude stabilization. Five Magnetorquers are utilized with the BDot detumble law to damp oscillations about the equilibrium attitude. Deploying or retracting all booms simultaneously varies the aerodynamic drag force experienced by the satellite without upsetting the attitude stability.

A six degree of freedom attitude and orbit propagator was developed to asses the attitude

stability of the D3 system and make design decisions about the system geometry. This propagator characterized the satellite state at each point in time by a 13 element vector containing the attitude quaternion, angular velocity, spacecraft position, and translational velocity. Knowledge of the forces and torques applied to the spacecraft were used to compute the derivative of the state vector at each time step which enabled the determination of the satellite state at all points in time using standard numerical integration techniques. While this method of simulation is commonly used in aerospace applications, there are numerous different conventions for defining quaternions, reference frames, and state vector components. As such, the implementation details of the simulation environment and the modeling of the attitude and orbital dynamics are discussed in the appendix.

This paper begins with a summary of the D3 system objective. The analysis and hardware design presented in the rest of the paper is geared toward the fulfillment of these objectives. Section III discusses the modeling of the passive environmental forces and torques acting on the spacecraft that were taken into account in the simulation. The proposed implementation of the popular B-Dot magnetorquer de-tumble law is discussed in section IV. Though many possible system configurations where tested using the simulation and control framework established up to this point, only the simulations results corresponding to the final system design are presented in section V. These simulation results show that the system meets or exceeds the performance requirements and lay the foundation for the physical hardware design discussed in Section VI. Section VII includes thermal simulations verifying that the proposed hardware will assume acceptable temperature profiles. Section VIII presents the conclusions reached during the simulation and hardware design process.

II. System Requirements

In order to be used as a reliable, low-cost attitude and orbit control system on a variety of LEO small satellite missions, the D3 system was designed to meet the following requirements.

- The D3 shall weight less than 1 kg and occupy a volume of less than 1U (10 x 10 x 10 cm)
- The D3 shall be made easy to integrate into a standard CubeSat structure and the external dimensions of the device shall conform to the CubeSat standard.
- The D3 must be able to successfully de-orbit a 12U, 15kg spacecraft from 700km circular orbit

in under 25 years assuming standard atmospheric conditions.

- The D3 system must enable the spacecraft to maintain passive ram-alignment within 15 degrees up to an altitude of 700 km. This maximizes drag area in order to expedite de-orbit and provides a predictable drag profile for orbital maneuvering.
- The D3 must be fully retractable such that the aerodynamic profile of a CubeSat with the D3 retracted is identical to the profile of that CubeSat without the D3.
- Components of the D3 shall not create additional debris upon re-entry.
- All computing and control mechanisms required to operate the D3 shall be self-contained and capable of receiving commands from a CubeSat bus of compatible hardware
- Peak power must remain under 4W for 30 seconds.
- Angular momentum should not be transferred to the spacecraft from the D3 system during deployment
- The system must be able to handle at least 1,000 cycles of deploying and retracting without experiencing fatigue-induced failures

III. Environmental Forces and Torques

Gravitational, aerodynamic, and magnetic effects impart external forces and torques on the spacecraft. The external forces affect the translational motion of the spacecraft while the external torques affect the rotational motion. The accurate modeling of these forces and torques is necessary to compute the 13-element state derivative for use in a complete 6DOF simulation.

A. Aerodynamic Drag

Aerodynamic drag force is given by the equation [28]

$$\vec{F_d} = -\frac{1}{2} C_d \rho A v_\infty \vec{v}_\infty \tag{1}$$

where C_d is the drag coefficient, ρ is the density, A is a reference surface area, and $\vec{v}_\infty$ is the velocity vector of the spacecraft relative to the atmosphere. Eq. 1 can be divided by the spacecraft mass

and re-written to provide the acceleration due to drag

$$\vec{a_d} = -C_b \rho v_\infty \vec{v}_\infty \tag{2}$$

Where the ballistic coefficient C_b is given by

$$C_b = \frac{C_d A}{2m} \tag{3}$$

The greatest uncertainty in the drag force is associated with the drag coefficient and density, though models do exist for both. For completely specular reflection where particles do not interact with each other and where they reflect off the surface at the same angle at which they impact, the theoretical drag coefficient is two for a sphere and four for a flat plate perpendicular to the velocity vector if the area used for Eq. 1 is the area of the plate. The 1976 standard atmosphere [29] was used to calculate the density at various altitudes to characterize the behavior of the satellite under average orbital conditions. For a specific orbit, more advanced density models such as NRLMSISE-00 [30] can be utilized for increased accuracy. To model the total aerodynamic drag force and torque, the spacecraft can be discretized into a collection of flat plates where the quaternion relating each plate to the spacecraft body frame is known. The surface normal vector of each plate with respect to the satellite body frame can then be calculated based on the orientation quaternion of the plate. For all plates where the angle between the surface normal vector and the velocity vector is greater than 90 degrees (surface is exposed to the air-stream), the component of the velocity vector perpendicular to the plate ($V_\perp$) can be calculated and used with Eq. 1 to calculate the aerodynamic drag force acting on the plate. This force can be assumed to act at the geometric center of the plate and opposite the direction of the surface normal vector. The vector from the satellite's center of mass to the panel's geometric center can be crossed with the aerodynamic force to calculate the aerodynamic torque acting on the spacecraft due to this panel. The aerodynamic forces generated by all the panels can be summed to calculate the total aerodynamic force acting on the satellite. Similarly, the aerodynamic torques caused by each panel can be added to calculate the total aerodynamic torque acting on the satellite.

Note that this method of aerodynamic modeling does not take into account the occlusion of some panels by other panels. Techniques have been developed to account for occlusion [31], but

they were not implemented in this work because the geometry of the spacecraft (discussed later) was such that occlusion was not a significant factor in the total aerodynamic force and torque.

B. Gravitational Effects

The Earth's gravity is by far the dominant force acting on a spacecraft in low Earth orbit. Solar and lunar gravity do have an effect but that effect is negligible for LEO spacecraft and is not considered here. If the Earth is assumed to be a point mass, the spacecraft's acceleration due to gravity is given by [32]

$$\vec{a}_g = -\frac{\mu}{r^3}\vec{r} \tag{4}$$

In reality, Earth is closer to on oblate spheroid than a point mass resulting in the J2 perturbation which, while several orders of magnitude smaller than two-body gravity, is several orders of magnitude greater than the next largest environmental perturbation. Let the vector from the center of Earth to the spacecraft center of mass expressed in the ECI frame be denoted as

$${}^E\vec{r} = \left[{}^E x\, {}^E y\, {}^E z\right]^T \tag{5}$$

The acceleration due to gravity including J2 is given by Bate, Muller, and White [33] as

$${}^E\ddot{x} = -\frac{\mu\, {}^E x}{r^3}\left[1 - \frac{3}{2}J_2\left(\frac{R_e}{r}\right)^2\left(\frac{5\, {}^E z^2}{r^2} - 1\right)\right] \tag{6}$$

$${}^E\ddot{y} = \frac{{}^E y}{{}^E x}\, {}^E\ddot{x} \tag{7}$$

$${}^E\ddot{z} = -\frac{\mu\, {}^E z}{r^3}\left[1 + \frac{3}{2}J_2\left(\frac{R_e}{r}\right)^2\left(3 - \frac{5\, {}^E z^2}{r^2}\right)\right] \tag{8}$$

For any spacecraft that is not a point mass, there will be some parts of the spacecraft that are closer to the Earth than others for any given attitude. The parts closer to Earth will experience a greater gravitational attraction resulting in a difference between the center of gravity and center of mass. This difference means that the gravitational force will exert a torque about the center of mass, causing the spacecraft to rotate. This is known as gravity gradient torque and can be written in terms of the spacecraft principal moments of inertia and the spacecraft position vector as [32]

$$
\begin{aligned}
{}^{B}M_x &= \frac{3\mu^B y^B z}{r^5}\left(I_{zz} - I_{yy}\right) \\
{}^{B}M_y &= \frac{3\mu^B x^B z}{r^5}\left(I_{xx} - I_{zz}\right) \\
{}^{B}M_z &= \frac{3\mu^B x^B y}{r^5}\left(I_{yy} - I_{xx}\right)
\end{aligned} \tag{9}
$$

Note that x, y, and z are the components of the spacecraft position vector expressed in the satellite body frame and M_x, M_y, M_z are the components of the gravity gradient torque vector expressed in the body frame.

C. Magnetic Hysteresis Torques

Ferromagnetic components onboard a spacecraft spacecraft can easily become magnetized by the Earth's magnetic field. These components retain some of their magnetization as the spacecraft changes attitude and can interact with the Earth's magnetic field to produce a torque. This is known as magnetic hysteresis torque. Often, spacecraft with no active attitude control include hysteresis rods (long ferromagnetic rods) to reduce the spacecraft's rate of tumble. While properly sized hysteresis rods can reduce the steady state tumble rate, the hysteresis effect is not comparable to that of a viscous damper. Hysteresis torques sometimes add angular momentum to the spacecraft and sometimes remove it. However, the amount of angular momentum removed, on average, tends to be more than the angular momentum added when above a certain angular velocity threshold. Below this threshold, the hysteresis torques will act as a disturbance and perturb the spacecraft's attitude. For systems such as this one with long booms, making these booms out of a ferromagnetic material could cause significant hysteresis torques which may result in undesired effects. While the fundamental physics behind magnetic hysteresis is not extremely well known, there are some mathematical techniques (based on experimental data) that can be utilized to characterize the hysteresis effects on a satellite and determine which materials to use.

The induced magnetic flux density in a metallic rod that has been exposed to some external sinusoidally varying magnetizing field is given by the hysteresis loop shown in Figure 2 which was taken from the NDT Resource Center [34]. When initially demagnetized and exposed to some external magnetizing field H (measured in Amps/meter), the magnetic flux density B (measured

in Telsa) in the rod increases until it reaches its saturation value B_s (point a on the diagram). H must then be decreased to the coercivity point H_c (point c on the diagram) for B to become zero again. If H is reduced to zero, the rod will still retain some magnetic flux density value B_r (magnetic remanence) given by point b on the diagram. Reducing H beyond H_c decreases B until the saturation point $-B_c$ (point d). The cycle continues if H is increased again. The magnetic hysteresis properties of a material can be completely specified by H_c, H_r, and B_s. Note that when the term "magnetic field" is used, the B-field is what is often referred to although "magnetic field" has been traditionally reserved for H. As such, B will refer to the magnetic flux density and H will refer to the external magnetizing field for the purposes of hysteresis torque calculation. Magnetic field models such as the International Geomagnetic Reference Field (IGRF) [35] generally return the value of the B. B can be converted to H for use in hysteresis calculation by

$$B = \mu_0 H \tag{10}$$

where μ_0 is the permeability of free space.

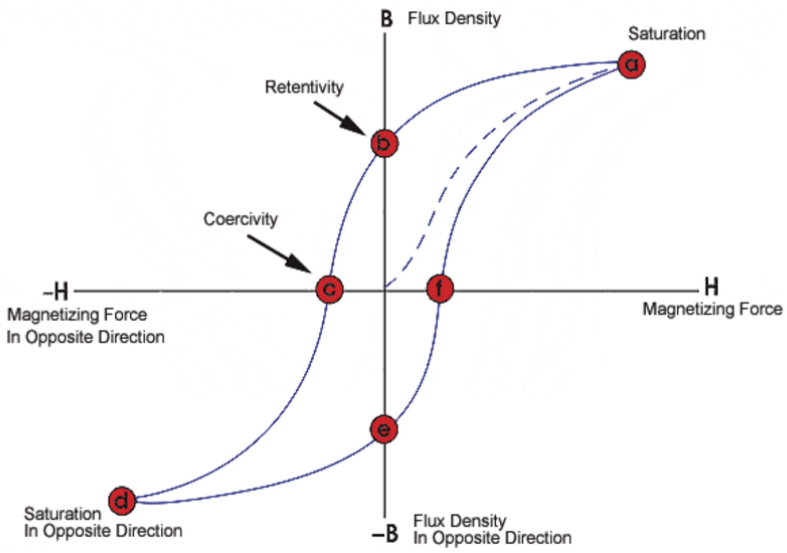

Fig. 2 Magnetic Hysteresis Loop

Flatley and Henretty[36] found the *arctan* function to be a good fit to the hysteresis loop based on experimental data. The left boundary of the hysteresis loop can approximated by

$$B = \frac{2}{\pi} B_s \tan^{-1}\left[k(H + H_c)\right] \tag{11}$$

where B_s, B_r, and H_c are the saturation, remanence, and coercivity of the material in question and

$$k = \frac{1}{H_c} \tan\left(\frac{\pi B_r}{2B_s}\right) \tag{12}$$

The right boundary of the hysteresis loop is similarly modeled by

$$B = \frac{2}{\pi} B_s \tan^{-1}\left[k(H - H_c)\right] \tag{13}$$

The slope of the boundary curve (either boundary) can be found by solving Eq. 11 for H, calculating the derivative with respect to H and then solving for dB/dH [36]. This yields

$$B' = \left(\frac{dB}{dH}\right)_{bound} = \frac{2}{\pi} k B_s \cos^2\left(\frac{\pi B}{2B_s}\right) \tag{14}$$

Note that this value of dB/dH is applicable only if the current value of B lies along the boundary of the hysteresis loop. There are many cases where B may not lie along this boundary such as when the simulation first starts with $B = 0$ and when the maximum value of H is not large enough to drive B all the way up to the saturation value of B_s. In this case, the actual value of dB/dH can be calculated based on the boundary slope (B') and the fractional distance from the corresponding boundary (f).

$$\frac{dB}{dH} = \left[q_0 + (1 - q_0) f^p\right] B' \tag{15}$$

where q_0 and p are empirically determined constants calculated to fit the experimental data and

$$f = \frac{|H - H_L|}{2H_c} \tag{16}$$

If dH/dt is positive, the right boundary H_r is used in Eq. 16, while if dH/dt is negative, the left boundary H_L is used in 16. With the ability to calculate dB/dH for any values of H and B, the time rate of change of the magnetic flux density induced in the boom can be calculated as

$$\frac{dB}{dt} = \frac{dB}{dH}\frac{dH}{dt} \tag{17}$$

dH/dt can be calculated by first determining the rate of change of H in the satellite body frame and taking the dot product of that vector with the vector along the boom axis. In addition to the

attitude quaternion and ECI position and velocity vectors, the overall state vector in the simulation can be expanded to contain the magnitude of the magnetic flux density along each boom. The above procedure can be used to calculate dB/dt at each point in time. To simulate magnetic hysteresis, the state vector can be augmented to contain the current value of B for each boom during the numerical integration. For each boom, the magnetic moment vector can be calculated as

$$\vec{\mu} = \frac{BV\vec{l}}{\mu_0} \tag{18}$$

where V is the volume of the boom, $\vec{l}$ is the vector along the length of the boom and μ_0 is the permeability of free space. The magnetic moments of all the booms can be summed and the total magnetic hysteresis torque can than be calculated by

$$\vec{T}_{hyst} = \vec{\mu}_0 \times \vec{B}_{Earth} \tag{19}$$

Where B_{Earth} is the magnetic field (flux density) of the Earth given directly by the IGRF model [35].

IV. Active Attitude Control using Magnetorquers

When satellites are initially deployed, they generally experience some initial angular velocity and are in a "tumbling" state. To eliminate this initial angular velocity, external torques must be applied to the satellite. A popular way to do this is with magnetorquers which are electromagnets that can interact with the Earth's magnetic field to produce desired torques. Note that the magnetic field discussed here is the magnetic flux density measured in Tesla (not to be confused with the H-field). Since the currents flowing through the magnetorquers can be actively controlled, it is possibly to ensure that the resulting magnetic torque is always in the direction that reduces the overall spacecraft angular momentum as much as possible. This can be accomplished using the popular B-Dot de-tumble law[27].

A. BDot De-tumble Law

The magnetic moment vector generated by a magnetorquer is given by [37]

$$\vec{\mu} = IAn\hat{s} \tag{20}$$

where I is the current running through the magnetorquer, A is the area, n is the number of turns, and $\hat{s}$ is the vector normal to the coil measured in a right-handed sense such that the fingers of a right hand curl along the direction of the current if the thumb is pointing along $\hat{s}$. Assuming three orthogonal magnetorquers, a total magnetic moment vector can be created in any direction. Since magnetic torque involves a cross product of the magnetic field vector, the magnetic torque must be perpendicular to the magnetic field vector. Since magnetic torque is given by Eq. 19, the set of possible commanded magnetic moments will be restricted to values of $\vec{\mu}$ perpendicular to $\vec{B}_E$ (the magnetic field of Earth) in order to maximize the resulting torque. Selecting the direction of $\vec{\mu}$ perpendicular to the satellite angular velocity $\vec{\omega}$ along the $\vec{\omega} \times \vec{B}_E$ vector ensures that the angle between the torque vector and the projection of $\vec{\omega}$ onto a plane perpendicular to $\vec{B}_E$ will be 180 degrees as shown in Figure 3. For a given magnitude of $\vec{\mu}$, this direction generates a torque vector that will serve to reduce the overall spacecraft angular momentum more than would the torque vector generated by placing $\vec{\mu}$ along any other direction. The total magnetic moment vector associated with the B-Dot law can be calculated as:

$$\vec{\mu}_{tot} = -k\dot{\vec{B}}_E \tag{21}$$

where k is a constant gain selected based on the strength of the magnetorquers and the desired performance and $\dot{\vec{B}}_E$ is the time rate of change of the magnetic field vector as observed in the satellite body frame given by

$$\dot{\vec{B}}_E = \frac{^E d\vec{B}_E}{dt} = \vec{B}_E \times {}^E\vec{\omega}^B = \frac{\vec{B}_{E2} - \vec{B}_{E1}}{\Delta t} \tag{22}$$

In some implementations, the unit vector in the $\dot{\vec{B}}$ direction is used in Eq 21, but the system will remain stable and effectively de-tumble the satellite either way. Unlike magnetic hysteresis torques, active magnetic control using B-Dot does act similarly to a velocity damper and can reduce the total spacecraft angular velocity to a very low final value (around 2 rotations per orbit in practice).

An aerodynamic or gravity gradient stabilized satellite with no active damping will oscillate like an undamped pendulum about the equilibrium point. In addition to de-tumbling the satellite, the

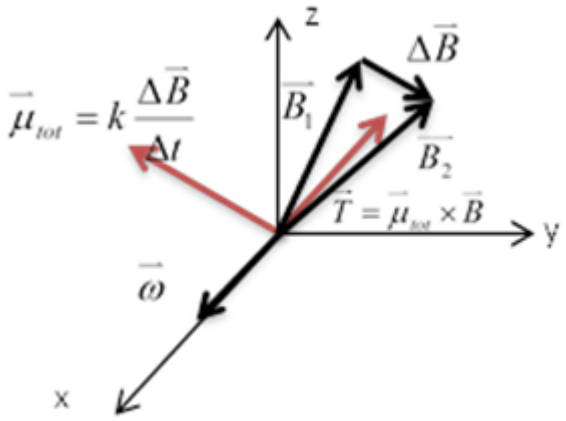

Fig. 3 Magnetic Moment and Torque from B-Dot Detumble Law [38]

B-Dot law can also be employed as a velocity damper to reduce the amplitude of these oscillations and minimize the steady state pointing error.

B. Implications of using Active Control

Any use of active attitude control adds a measure of risk and complexity to the system. However, the simplicity and robustness of the B-Dot algorithm make it easy to implement with minimal risk.

In order to sense the magnetic field vector in the body frame, the spacecraft must contain at least one 3-axis magnetometer. Magnetometers consume power and are susceptible to damage due to launch vibrations and thermal cycling. In addition to measurement noise, magnetometers can also exhibit bias errors due to thermal effects and the magnetic fields generated by the satellite electronic. Magnetorquers must be turned off while taking magnetometer measurements. A benefit of the B-Dot algorithm, however, is that since it relies on subtracting two magnetic field measurements over time, the bias errors cancel. This eliminates the need for complicated models of the magnetic fields created by the satellite electronics. Multiple magnetometers can also be hosted on the spacecraft to minimize the effects of a single magnetometer failure. The magnetorquers themselves are solid state components (no moving parts) and thus are far less likely to fail than attitude control actuators such as reaction wheels or control moment gyros. However, there is always a risk of a short circuit developing in a coil or the failure of a magnetorquer driver chip although these failure modes are very rare compared to other types of failures that can happen on a spacecraft. Magnetorquers also

require power, but beyond the initial detumble that is generally complete within 24 hours, the total magnetorquer power consumption needed to continuously run the B-Dot law is generally only a few milliwatts.

Overall, the B-Dot is one of the simplest (if not the simplest) attitude control algorithm, and the risks associated with the active control are minimal compared to the benefits and are far lower than the risks associated with conventional reaction wheel based attitude control systems.

V. Design Analysis and Simulations

Two goals of D3 were to facilitate the de-orbit of a 12U spacecraft from 700 km in 25 years and to provide a ram-aligned spacecraft attitude in order maximize the surface area perpendicular to velocity and follow a predictable drag profile. The D3 also required the ability to deploy and retract in order to perform orbital maneuvers through variations in the aerodynamic drag force. Using the aforementioned modeling techniques, simulations were conducted to determine the drag device surface area required to meet the 25 year de-orbit time requirement and to assess the ability of the drag device to maintain the spacecraft in a ram-aligned attitude. A method of partially deploying some of the booms to achieve 3-axis attitude stabilization using aerodynamic and gravity gradient forces was also investigated via simulations.

A. Orbit Lifetime Analysis

The orbit lifetime of a spacecraft in LEO is directly related to the amount of aerodynamic drag the spacecraft experiences. If a spacecraft with some ballistic coefficient C_{b1} (as defined in Eq. 3) requires some amount of time Δt_1 to de-orbit, the de-orbit time Δt_2 for another spacecraft with the same initial conditions but a different ballistic coefficient can be estimated by

$$\Delta t_2 = \frac{C_{b1}\Delta t_1}{C_{b2}} \tag{23}$$

Eq. 23 is very powerful because it allows the orbit lifetime for various satellite configurations to be estimated after conducting a single orbital simulation. Eq. 23 is proven in this author's previous work for circular orbits where density is a function of semi major axis [39]. The proof can be summarized as follows. From the gauss variational equations given in Eq. 9-24 of Vallado's book

[28], the rate of change of semi major axis with respect to time can be derived for a circular orbit as

$$\frac{da}{dt} = \frac{2a_d}{n} = 2a_d\sqrt{\frac{a^3}{\mu_e}} \tag{24}$$

where a if the semi major axis, μ_e is Earth's gravitational parameter and a_d is the acceleration due to aerodynamic drag given by Eq. 2. substituting Eq. 2 and Eq. 3 into Eq. 24, assuming that the orbital velocity is equal to the velocity relative to the atmospheric particles, and re-arranging yields

$$-\sqrt{\frac{\mu_e}{a^3}}\left(\frac{1}{2C_b\rho v^2}\right)da = dt \tag{25}$$

The velocity magnitude in a circular orbit is given by

$$v = \sqrt{\frac{\mu_e}{a}} \tag{26}$$

Substituting Eq. 26 into Eq. 25, multiplying both sides of the equation by C_b, and integrating yields

$$\Delta t C_b = \int_{a_0}^{a_f} -\frac{da}{2\sqrt{\mu a}\rho} \tag{27}$$

This equation represents the time required for the orbit to decay from some initial to final semi major axis value. If density is a function of semi major axis, then all terms inside the integral are functions of semi major axis, and the solution to the integral will likewise be a function of a. As a result, the product $\Delta t C_b$ will be a function of only the final and initial semi major axes. If we consider F to be the solution to the integral, then

$$\Delta t C_b = F(a_f) - F(a_0) \tag{28}$$

Since de-orbit from a given set of initial conditions can be defined as some change in semi major axis, Eq. 28 shows that product $\Delta t C_b$ is constant for a given initial semi major axis. This leads directly to Eq. 23.

To approximate the orbit lifetime for various initial circular orbit altitudes, a single trajectory was propagated until de-orbit from an 800 km orbit with $C_{b_{sim}} = .1333\frac{m^2}{kg}$ assuming a spherical Earth and 1976 standard atmosphere for density calculations. In reality, the Earth is not a perfect sphere and the density at each altitude is not fixed, but these assumptions provide a good benchmark for high level analysis. After propagation was complete, Eq. 23 was utilized to estimate the orbit

lifetimes for satellites with different ballistic coefficients. Starting the simulation from 800 km provided the orbit lifetime for all initial circular orbit altitudes at and below 800 km.

To calculate the area of a drag device needed to de-orbit a 12U (15 kg) spacecraft from 700 km in 25 years, Eq. 23 was first utilized to calculate the C_b needed to de-orbit from an altitude of 700 km. Given the simulated orbit lifetime of a spacecraft initially in a 700 km altitude circular orbit with $C_{b_{sim}}$, the required C_b value was

$$C_{b_{req}} = \frac{C_{b_{sim}} \Delta t_{sim}}{25\ years} = \frac{(.1333)(6.25)}{25} = .0333 \tag{29}$$

The drag coefficient of a spacecraft in free molecular flow with completely specular reflection will range from 2 for a sphere to 4 for a flat plate [40]. Assuming a drag coefficient of two as a conservative estimate, the surface area of the drag device needed to achieve a C_b of .0333 for a 15 kg spacecraft can be calculated from Eq. 3 as

$$A_{req} = \frac{2C_b m}{C_d} = \frac{2(.0333)(15)}{2} = .5m^2 \tag{30}$$

From Eq. 30 the desired drag area for the fully deployed D3 was $.5m^2$ and the system was designed accordingly. To better illustrate the expected performance of the D3 on a variety of platforms, Figure 4 displays the orbit lifetime vs. initial altitude for spacecraft with ballistic coefficients corresponding to various geometries with and without the drag device. Included are orbit lifetimes for 12U, 6U, 3U, and 2U satellites weighing 15, 8, 4, and 2 kg respectively and equipped with the drag device (area of $.5m^2$). Also included are orbits lifetimes for 12U and 1U-6U spacecraft with no deployables oriented with their largest faces perpendicular to velocity. Note that the drag coefficient of all spacecraft was assumed to be two as a conservative estimate. While 25 years were required for the 12U (15 kg) spacecraft to de-orbit from 700 km, satellites weighing under 15 kg de-orbited much more quickly and could be deployed at higher altitudes. The 3U spacecraft was able to de-orbit from over 800 km in under 25 years. Figure 4 verifies that a spacecraft with $C_b = .0333$ de-orbits in 25 years if it begins in a 700 km circular orbit. Overall, the D3 significantly reduces the orbit lifetime of nearly any legacy CubeSat configuration.

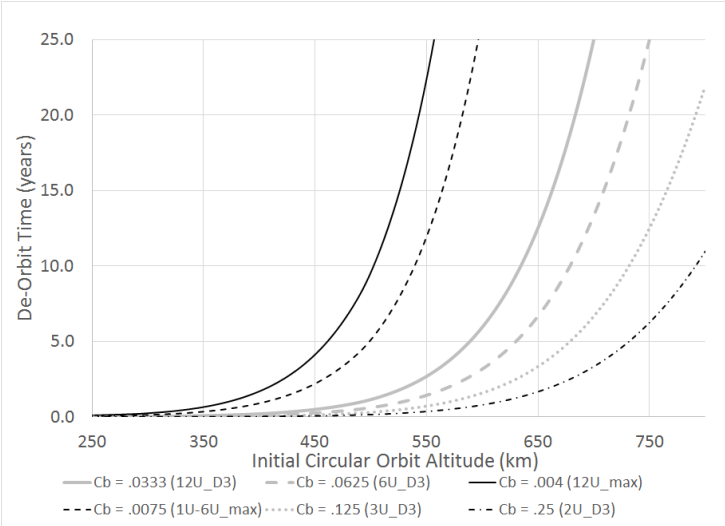

Fig. 4 Orbit Lifetime vs. Initial Circular Orbit Altitude

B. Attitude Dynamics Simulations and Results

To keep the spacecraft in a ram-aligned attitude so that the area perpendicular to the velocity vector would be maximized, a drag device with four 3.7 meter long, four centimeter wide measuring-tape-style deployable booms inclined at 20 degrees relative to the rear face of the satellite was decided upon. The booms would be deployed by a stepper motor and retracted by running the motor in the opposite direction. The boom geometry is shown in Figure 10 and the hardware specifications are detailed in Section VI. This configuration provided a total deployed area of $.5m^2$ and provided aerodynamic stability up to an altitude of 700 km. Simulation results showed that making the boom angle less than 20 degrees significantly reduced stability without appreciably increasing the surface area, while for angles greater than 20 degrees, the decrease in surface area was not justified by the slight increase in stability. As an added bonus, some of the booms could be partially deployed or retracted to create a clear spacecraft minimum moment of inertia axis that would align with the nadir vector due to gravity gradient torques. The non-magnetic Austenitic 316 stainless steel was selected as the material for the booms because hysteresis effects were deemed to be excessively large with ferromagnetic booms. The drag device will also contain a magnetometer and five magnetorquers in order to de-tumble the spacecraft and damp attitude oscillations using the B-Dot de-tumble controller. Discussed below are the results of the various simulations that

substantiated these decisions.

1. Detumble Phase

The first simulation conducted included torque due only to the B-Dot de-tumble controller. The satellite was assumed to have an initial tumble rate of 5 rotations per minute with the booms retracted. Only magnetic torques were considered in this simulation which represents the expected behavior of the satellite when B-Dot is activated after initial deployment into space, prior to the extension of the booms. The IGRF magnetic field model of the Earth [35] was used and provided the value of the magnetic field at each time step based on the spacecraft position. Using B-Dot alone, it was possible to get an angular velocity under .02 rpm within 12 hours. In practice, B-Dot would remain active until the spacecraft was below a certain angular velocity threshold before deploying the booms. Figure 5 illustrates the satellite angular velocity over time when running B-Dot and the magnetorquer power consumption. The pointing error is defined as the angle between the satellite long axis and the velocity vector. This errors oscillates randomly because there are no aerodynamic torques to align the satellite with the velocity vector. Figure 6 shows the zoomed in angular velocity in order to illustrate the steady state performance of the B-dot law. Note that the magnetorquer power consumption after the initial detumble was almost zero.

2. Simulating Aerodynamic Stabilization

The next simulation included magnetic torque from the B-Dot algorithm, aerodynamic torques corresponding to all boom fully deployed, and gravity gradient torques corresponding to all booms fully deployed. This simulation provides a good indication of the expected system performance with non-ferromagnetic booms. Figure 7 illustrates the stability of the system when aerodynamic and gravity gradient torques are applied for booms deployed at a 20 degree angle relative to the rear face of the satellite. The deployed booms make the spacecraft behave similarly to a dart or an arrow by placing the center of pressure behind the center of mass. This means that if the satellite is perturbed from it's ram-aligned configuration, an aerodynamic restoring force will try to re-align it with the

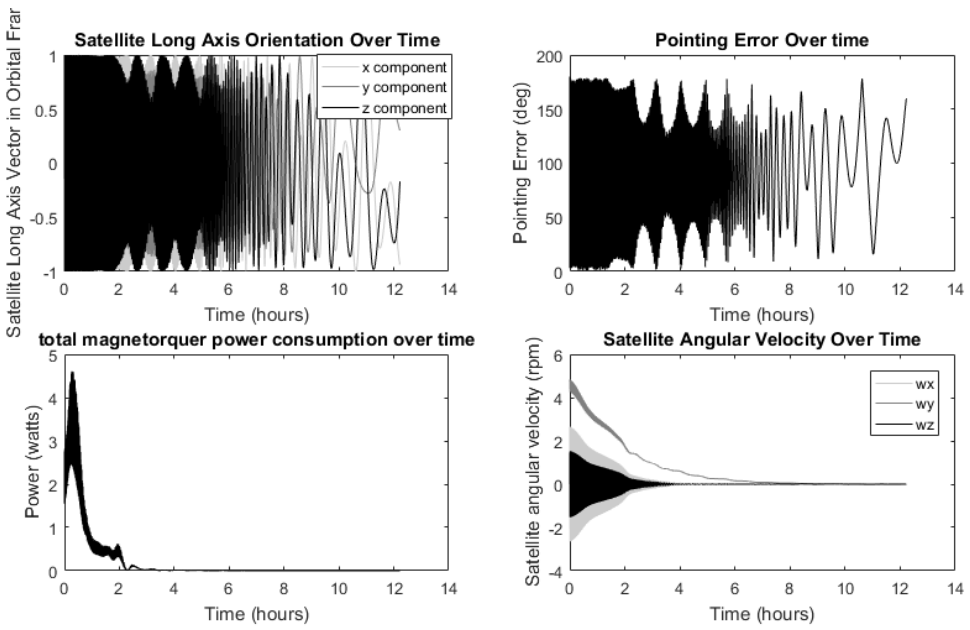

Fig. 5 B-Dot Only in 700 km Circular Orbit

velocity vector. With the booms fully deployed, the z-axis of the satellite (axis going through center of drag device) is the maximum moment of inertia axis. Gravity gradient torques work to align the minimum moment of inertia axis with the nadir vector, so this means that the maximum moment of inertia axis must be perpendicular to the nadir vector; a constraint which helps maintain ram-alignment. Though the roll axis is not constrained, both gravity gradient and aerodynamic torques work to keep the satellite aligned with the velocity vector while the magnetorquers help damp oscillations in the attitude.

3. Simulating Magnetic Hysteresis

The system from Section V B 2 was simulated with the inclusion of hysteresis torques due to the potential magnetization of the booms. Figure 8 demonstrates the hysteresis effects on booms made of wrought iron (one of the most ferromagnetic materials). As shown in the figure, the hysteresis torques dominate the aerodynamic and gravity gradient torques and result in system instability. This behavior is consistent with conclusions reached by other researchers through analyses and flight demonstrations that while hysteresis torques can help reduce the initial rate of tumble, they act as disturbances in the steady state [41, 42]. Additionally, the existing models for hysteresis

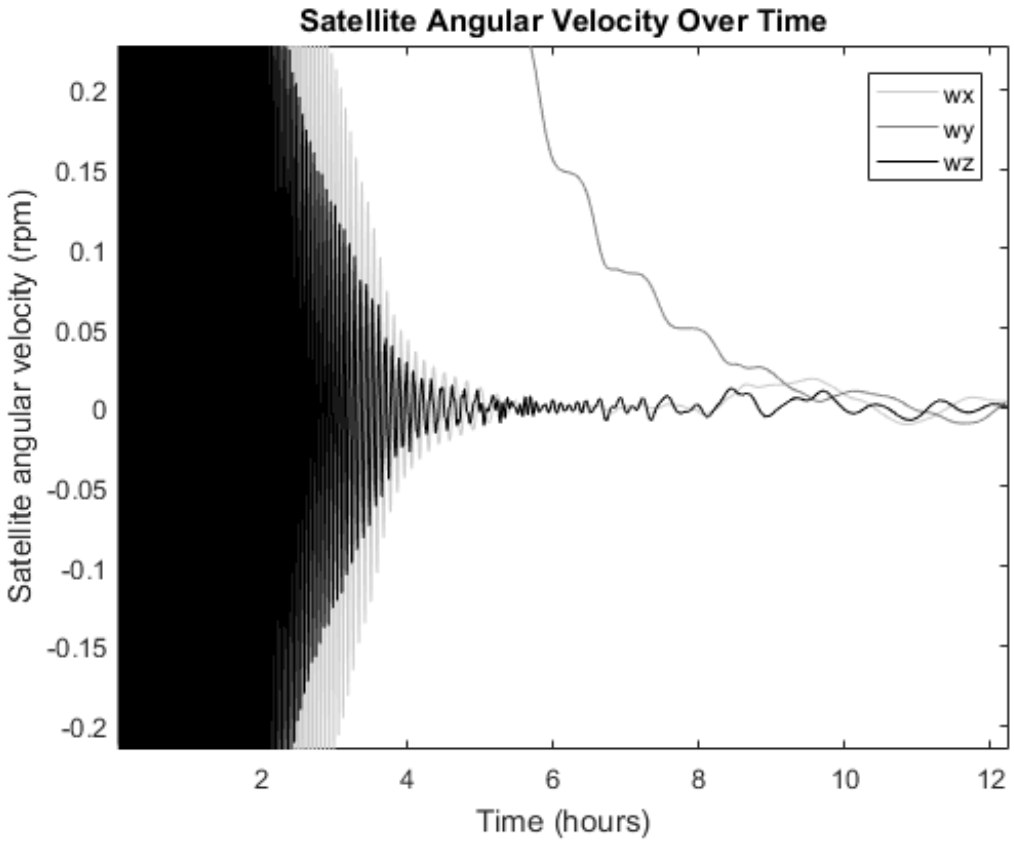

Fig. 6 Angular Velocity when Simulating B-Dot Torques Only in 700 km circular orbit

torques were based on experimental data for rods exposed to sinusoidally varying magnetic fields. Since there are 4 booms and they are more like rectangular prisms than rods, it is possible that the model does not provide an accurate depiction of how they will really behave. For these reasons, it was decided that the booms should be made of a non-magnetic material if possible to avoid the problems associated with unwanted hysteresis torques. Austenitic 316 stainless steel was decided upon due to its ductility, low melting point compared to other brands of stainless steel, and non-magnetic properties.

4. Three Axis Stabilization using Aerodynamic and Gravity and Gradient Torques

An added benefit of having retractable booms is the ability to align one axis of the satellite with the nadir vector using gravity gradient torques. By having two booms that are opposite each other partially deployed and having the remaining two booms fully deployed, the spacecraft minimum

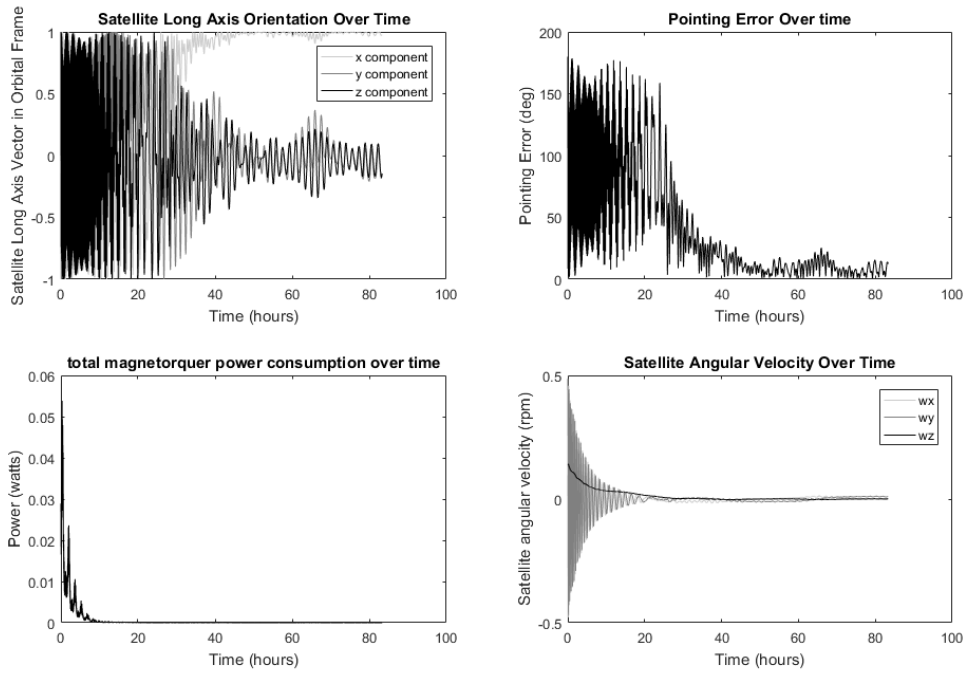

Fig. 7 Aerodynamics, Gravity Gradient, and B-Dot torques for Fully Deployed Drag Device in a 700 km Circular Orbit

moment of inertia axis (call it the y-axis) will be aligned with the two fully deployed booms. This axis will align with the nadir vector. With aerodynamic torques constraining the z-axis of the satellite to align with the velocity vector, the spacecraft will be 3-axis stabilized. This ability is useful if an antenna or science instrument needs to be pointing toward the ground (nadir), away from the ground (zenith), or toward the velocity vector. Figure 9 shows the attitude dynamics when two of the booms are deployed half way and the other two are fully deployed. Note that the graphs provide the components of each satellite body axis expressed in the orbital frame defined in the Appendix. Even with the reduction in aerodynamic torque, the spacecraft z-axis aligns with the velocity vector and the axis along the two fully deployed booms aligns with the nadir vector.

A drawback of gravity gradient stabilization is that configurations with the y-axis aligned with either the nadir or zenith vector will be stable. However, if the satellite stabilizes in the wrong orientation, it may be possible to roll the satellite by asymmetrically deploying the booms so that the minimum moment of inertia axis lies 45 degrees offset from the y-axis. The new stable orientation will have the y-axis offset 45 degrees from it's original orientation. After waiting for the attitude

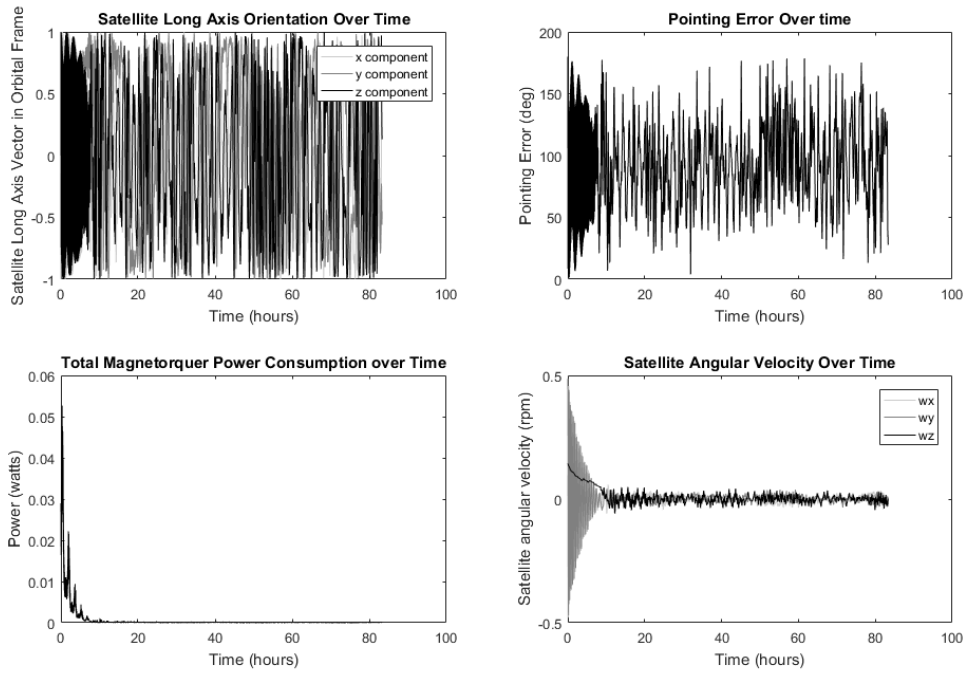

Fig. 8 Aerodynamics, Gravity Gradient, B-Dot, and Hysteresis Torques for Fully Deployed Drag Device in a 700 km Circular Orbit

to stabilize, another 45 degree rotation can be performed. The process can be continued until the spacecraft has been rotated 180 degrees to align the y-axis with the nadir or zenith vector as desired. Alternatively, if it is desired to align the y-axis with the nadir vector, the booms along the x-axis can first be fully deployed and the y-axis booms partially deployed such that the x-axis has minimum moment of inertia and aligns with the nadir/zenith vector. In that case, only two 45 degree rotations will be needed to align the y-axis with the nadir vector. The control logic by which the booms are deployed and retracted to properly align the satellite will be investigated in future work.

VI. D3 System Hardware

The D3 system was designed to be compatible with CubeSats and other small spacecraft. The system contains a 100mm x 100mm base to be able to easily mount to these spacecraft. The D3 was also designed to fulfill the requirements listed in Section II.

The drag area of $.5m^2$ required to de-orbit a 15 kg satellite from a 700 km circular orbit in 25 years is split over four independent drag-inducing booms. Each boom is therefore required to

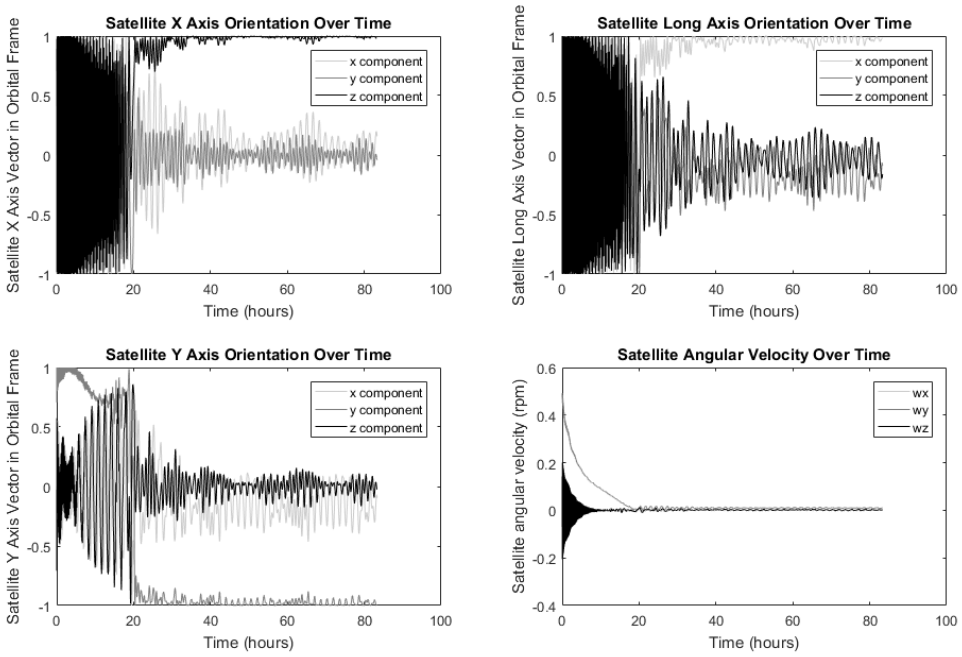

Fig. 9 3-axis Attitude Stabilization using Gravity Gradient and Aerodynamic Torques

produce a drag area of 0.125 m^2. This corresponded to 3.7m long booms if the booms are inclined at 20 degrees relative to the rear face of the satellite and the curved width of the booms is about 3.6 cm. This quadruple redundancy allows a limited modulation of the drag area even if three out of the four booms systems fail.

Each boom has a flat width of 4cm, and a length of 3.7m. The thickness is 0.127mm (0.005"). For the four booms, this results in a total boom volume of 75.2cm^3. A 10cm x 10cm x 5cm volume was used for the D3 system, as the full size was not needed. Assuming 90% of each dimension is available for interior space (i.e. accounting for wall space), the total available interior volume is 364.5cm^3. This results in approximately 21% of the interior volume being used for the actual booms. The remaining volume is used for other components, or left empty.

A. Booms Are Angled for Greater Stability

For aerodynamic stability, the booms are inclined at a 20 degree angle relative to the velocity normal, shown in Figure 10. As determined by simulations, increasing the angle would result in marginally more stability, at the cost of sharply increasing the required cross sectional area.

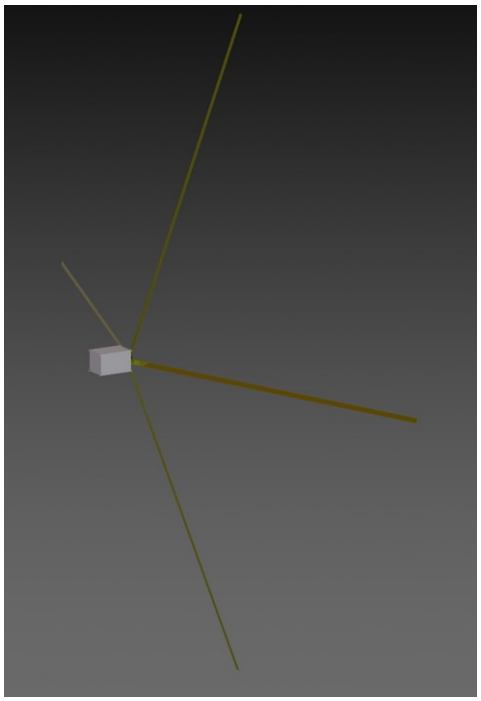

Fig. 10 Angling the Booms Backward Increases Stability

Conversely, decreasing the angle results in a sharp decrease in stability with only a marginal increase in cross wind area. The cross sectional area mentioned previously already takes into account the 20 degree angle. Section V elaborates further on the attitude stability properties.

B. Rolling is Used to Produce the Finished Shape

Because flat booms are not rigid enough to remain extended without curling or buckling, Nylon rollers are used to shape the booms. Three-point bending is used with the rollers to produce the desired cross section which looks very similar to the curved cross-section of a measuring tape boom. A male roller with a tip radius of curvature of 4mm is used to produce the desired shape. A female roller with curved edges holds the stock in place. The tip radius of curvature determines the finished geometry. By rolling with a tip radius of 4mm, the boom can be coiled without any creases in the center. Tip radii of 3mm and 2mm were also tested but were found to leave creases and could not be used. Adjusting the center-center distance of the rollers drives the bend angle. The geometry of the rollers is shown in Figure 11.

The booms assumed a V-shaped cross section with a rounded base after rolling. Since the booms exhibited spring-back after rolling, the radius of curvature did not remain at 4mm. Because

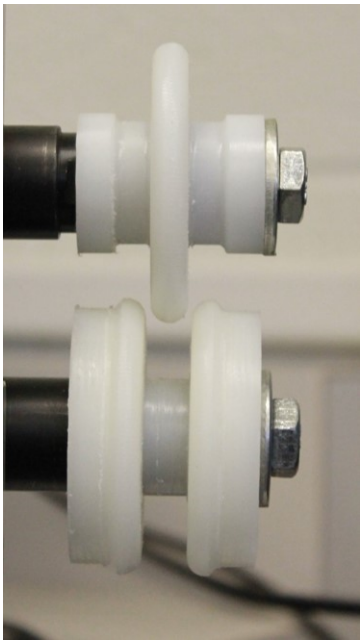

Fig. 11 Three-Point Bending Achieves the V-Shaped Cross Section

there was limited theory on exactly how much the rolled booms would spring back, multiple roller spacings were tested with the 4 mm radius roller until a boom was produced that had the desired curvature after spring-back. Using a V-shaped boom instead of a boom with a continuous curve as was initially intended led to easier manufacturing and an increased curved width for a given flat width and radius of curvature, shortening the required boom length. Figure 12 shows the difference in geometry between a continuously curved boom and a V-shaped boom. The team decided to continue using the designed boom length of 3.7m to increase the maximum drag area and ensure a sufficient drag area in the event of machining errors resulting in narrower booms.

C. Variation of Cross Sectional Area

Simultaneous coiling of all four booms is used to modulate the total drag area. To facilitate this coiling, each boom is attached to an aluminum drum. A twist-lock is used to secure the boom to the drum as shown in Figure 13, allowing for easy attachment and removal without the need for adhesives or welding. The tabs also allows some float, removing the need for tight tolerances.

The drum is driven by a Faulhaber AM1524 stepper motor with an attached 81:1 gearbox. The high reduction ratio ensures that the boom cannot backdrive the stepper, eliminating the need to

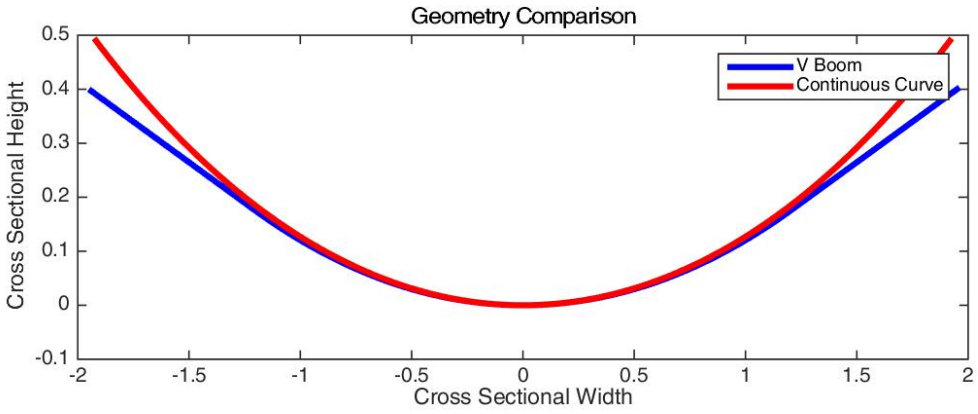

Fig. 12 V Boom Results in a Larger Cross Sectional Area

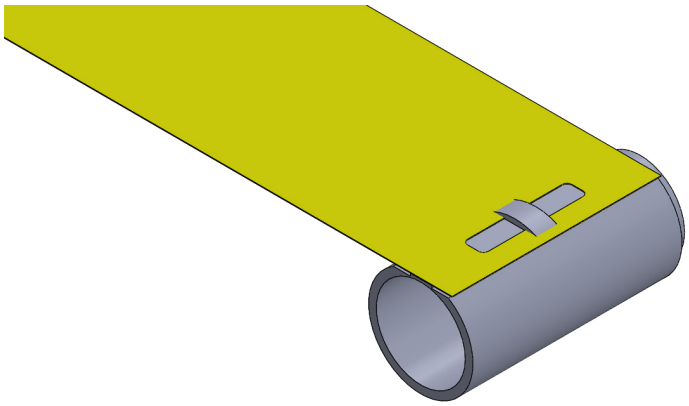

Fig. 13 The Booms Are Allowed to Float on the Drums

power the motor when the booms are not being deployed or retracted. Because the rotation of the stepper motor output shaft can be controlled precisely, a rotary encoder is not be necessary to measure boom deployment, greatly simplifying the system.

The base of the motor is fastened inside a sleeve, the base of which is then fastened to the outer shell as shown in Figure 14. The drum is then fitted over the sleeve, using a thrust roller bearing on each end to maintain alignment. The placement of the bearings over the drum is illustrated in Figure 15. Note that the drum contains a shoulder for mounting the bearing on the end closest to the motor shaft.

A second shell is used to hold the deployer assembly together. Four deployers are then attached to a base plate, spaced 90 degrees apart as shown in Figure 16. An expanded view of each deployer

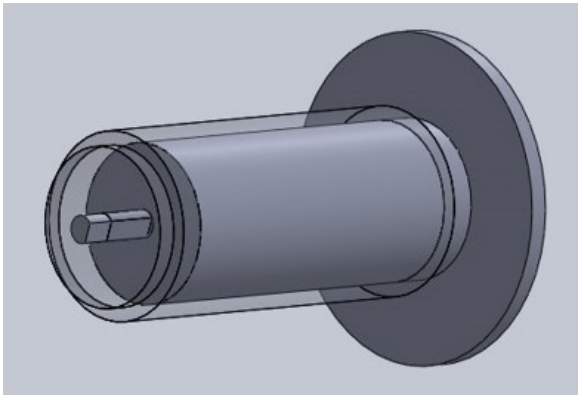

Fig. 14 Sleeve Attaches To Motor for Later Mounting

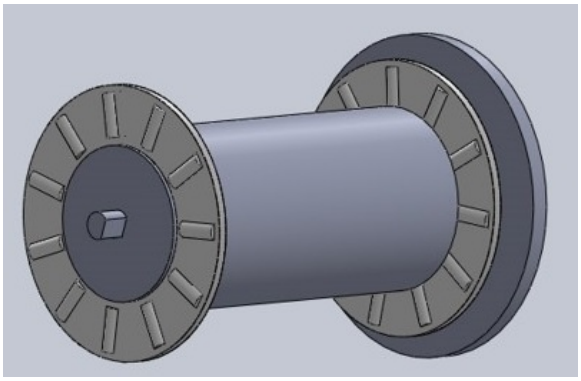

Fig. 15 Thrust Bearings Hold Drum In Alignment

assembly is shown in Figure 17.

Five magnetorquers in three groups are used for the B-Dot detumble law which reduces the overall satellite angular velocity. One magnetorquer is mounted on the end of each deployer and one is mounted on top of the deployer assembly as shown in Figure 18. Having at least three orthogonal magnetorquers allows any desired magnetic moment vector to be produced which is essential for the B-Dot controller. The current magnetorquer geometry allows for easier packing and redundancy in actuation if one of the deployer-mounted magnetorquers fails. A magnetometer will also be included in this system for measuring the ambient magnetic field.

An Intel Edison SoC (System-on-a-Chip) will control the hardware through driver chips and is capable of running algorithms for orbital maneuvering and de-orbit point targeting using aerodynamic drag. The latest version of the Edison contains a dual-core Intel Atom CPU clocked at 500 MHz and an Intel Quark microcontroller at 100 Mhz [43] and was previously used in the ScanSat [44]

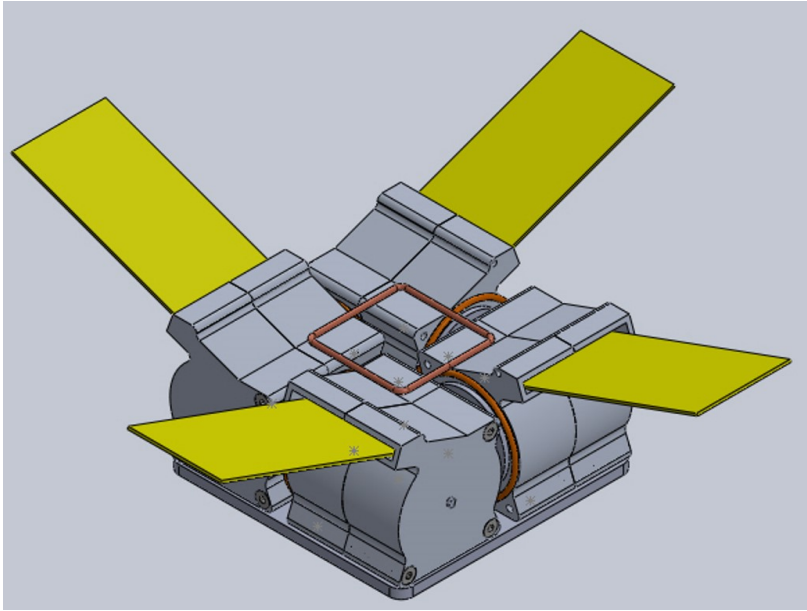

Fig. 16 Four Deployers Are Mounted to the Base Plate

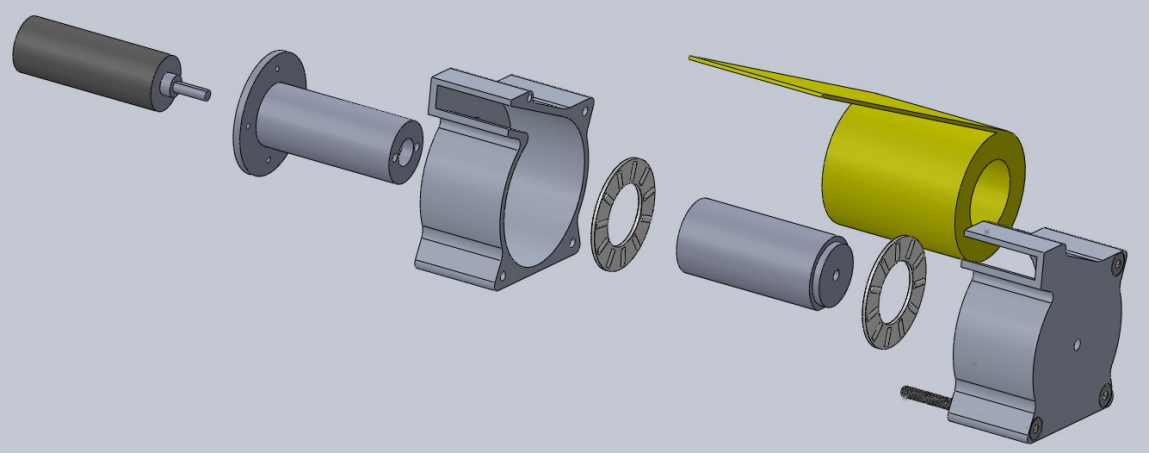

Fig. 17 Assembly of a Single Deployer

and CanSat [45] missions. The Atom CPU is used for computationally intensive maneuvering algorithms while the Quark can be utilized independently of the Atom for hardware control and simple guidance tracking algorithms. Though power consumption remains under 1.5W with all processors at full load, using only the Quark reduces power consumption to under 100 milliwatts.

Because of the reduced transistor count, the Quark is also expected to be less susceptible to cosmic radiation, making it preferable when limited computing power is needed. When the Atom processor is needed to run the computationally intensive maneuvering algorithms, the Quark will

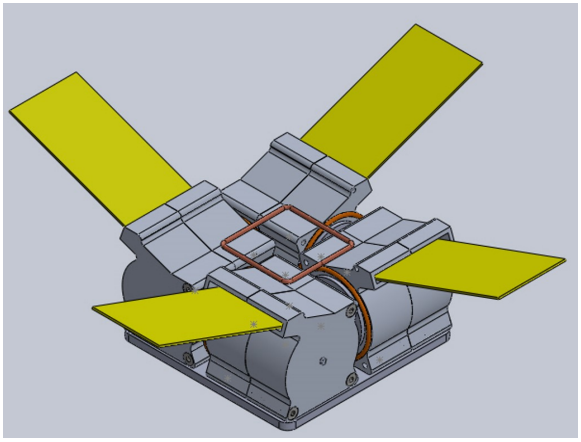

Fig. 18 Five Magnetorquers Provide Attitude Control

Fig. 19 Intel Edison Board, Image Courtesy Intel ®

serve as a watchdog timer, reseting the Atom if it does not receive a precisely timed "heartbeat" signal from the Atom. This will help return the system to operation if the Atom processor locks up due to a radiation-induced bit flip. The team is considering including an additional watchdog timer chip to reset the Quark processor if it locks up due to radiation-induced upsets. The Edison, watchdog timer chip, motor driver chips, magnetorquer driver chips, and magnetometers will all be located on a single printed circuit board that will attach to the drag device base plate.

When the spacecraft is initially deployed, the Edison SoC will first active the B-Dot magnetorquer de-tumble algorithm when commanded to begin operations by the primary spacecraft computer. When the spacecraft angular velocity is below a certain threshold, the Edison will fully deploy the booms while running the B-Dot detumble law to reduce oscillations in the attitude. Once the attitude has stabilized, the Edison will stop running the B-Dot law and will be ready to perform orbital maneuvering or targeted de-orbit algorithms by deploying and retracting the booms.

VII. Thermal Simulations

A. Thermal Simulations

After completion of the preliminary design, two Thermal Desktop ® simulations were used to determine the system's thermal profile. Different outer thermal coatings for the system components were considered to ensure an acceptable temperature range. A 500km altitude, 89 degree, sun synchronous orbit was used for the maximum heating case. This orbit will precess in such a way that the orbit angular momentum vector will always be aligned with the Earth-Sun vector, placing the satellite in continuous sunlight. A 500km equatorial orbit was used as the case with maximum thermal cycling, due to the large changes in solar heating as the satellite moves in and out of eclipse.

Some simplifications were used for the thermal model. Heat transfer between the D3 outer structures and the environment, and conduction through the D3 major structures have both been considered. Internal conduction inside the stepper, drum, and sleeve has not yet been considered. Table 2 shows the materials and surface treatments for the major parts of the system.

Table 2 D3 Materials and Optical Properties

Structure	Material	Surface Treatment	Solar Absorptivity	IR Emissivity
Shell	6061 Aluminum	None	0.44	0.143
Base	6061 Aluminum	None	0.44	0.143
Booms	316 Stainless Steel	None	0.39	0.11

The temperatures of the booms and shells for both sample orbits are shown in Figure 20. As expected, the sun-synchronous orbit showed a nearly constant temperature for both components, since the heat flux was nearly constant. In comparison, the equatorial orbit showed significant temperature fluctuations, especially for the booms, as the satellite passed into and out of eclipse.

Since the D3 system and accompanying spacecraft will have several computer boards, internal temperatures must be kept within the operating ranges of these boards. The component temperatures shown in Figure 20 would most likely result in the computer boards exceeding their operational limits and failing.

One solution to reduce the average temperatures is to anodize the aluminum components of the

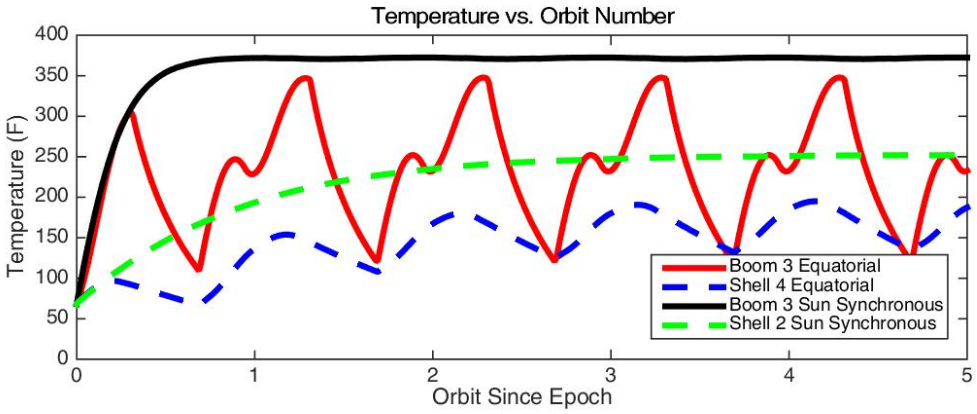

Fig. 20 Approximate Temperatures Experienced in Orbit

system, and add a Kapton® coating to the booms. The properties of these coatings are summarized in Table 3. Anodizing is an electrochemical process which can increase the emissivity of a material, leading to increased heat loss through radiation and a lower equilibrium temperature.

The Stefan-Boltzmann Law [46], shown below, allows one to calculate the heat leaving a body through radiation given the absolute temperature of the body (T), its radiating area (A_r) and its emissivity (ϵ).

$$Q_{out} = A_r \epsilon \sigma T^4 \tag{31}$$

The thermal radiation absorbed by the body is given by [46]

$$Q_{in} = A_p \alpha S \tag{32}$$

where $S = 1366 W/m^2$ is the solar constant, A_p is the area of the body perpendicular to the sun vector, and α is the body's absorptivity. An equilibrium temperature is reached when the solar radiation absorbed by the body is equal to the heat radiated out. This equilibrium temperature is calculated by setting Eq. 31 equal to 32 and solving for T.

$$T_{eq} = \sqrt[4]{\frac{S \alpha A_p}{A_r \epsilon \sigma}} \tag{33}$$

Because increasing the emissivity increases the heat radiated out of a body for a given temperature, anodizing a material will result in a lower equilibrium temperature since emissivity will be higher while absorptivity will remain roughly constant. Figure 21 shows the resulting temperature profile after the surface treatments.

Table 3 D3 Materials and Optical Properties After Surface Treatment

Structure	Material	Surface Treatment	Solar Absorptivity	IR Emissivity
Shell	6061 Aluminum	Anodized	0.44	0.56
Base	6061 Aluminum	Anodized	0.44	0.56
Booms	316 Stainless Steel	Aluminized Kapton	0.36	0.61

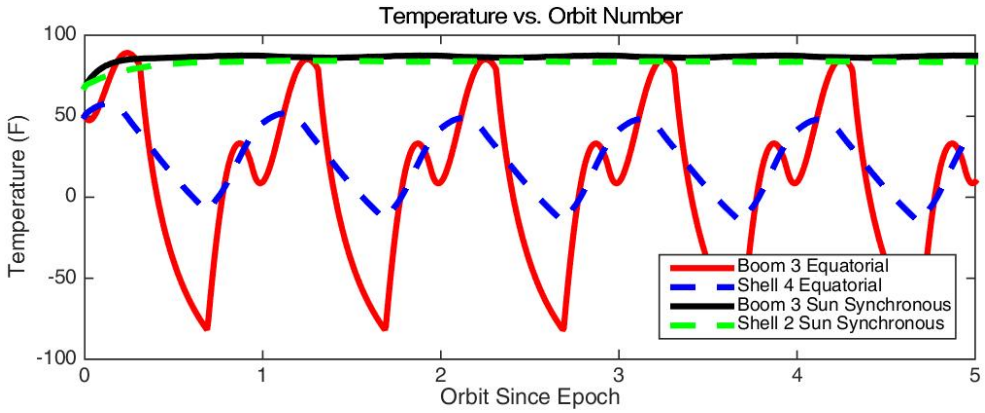

Fig. 21 Approximate Temperatures Experienced in Orbit, After Surface Treatment

B. Thermal Conclusions and Considerations

Preliminary simulations made it clear that launching the D3 with untreated aluminum and steel surfaces would result in excessively high temperatures and a rapid failure of the system. Fortunately, the use of surface treatments can reduce the equilibrium temperatures of the system components such that the thermal cycling that occurs each orbit does not cause the components to operate out of their acceptable temperature ranges. Anodizing the aluminum shells and coating the steel booms with Aluminized Kapton results in boom temperatures between about -80 and 80 degrees Celsius and shell temperatures between 0 and 80 degrees Celsius depending on the orbit. This range is acceptable for the D3 components. If extra mass is available, temperature fluctuations can be reduced by making the components thicker and increasing the thermal inertia. The board containing the Intel Edison and magnetorquer and motor driver chips will be thermally isolated from the outer structure to prevent excessive thermal cycling.

Additionally, the device is intended to burn up on re-entry such that no additional derbis is created. The D3 components with the highest melting points are the booms made of Austenitic

316 steel which will melt at around 1380 degrees Celsius. Utilizing a re-entry thermal analysis tool developed by the NASA Kennedy Space Center, it was determined that the booms and all other D3 components would disintegrate completely upon re-entry even if the booms were fully coiled.

VIII. Conclusions

Ultimately, it was determined that a cross-sectional area of $.5m^2$ was necessary to de-orbit a 12U (15 kg) CubeSat from 700 km in 25 years assuming standard atmospheric conditions. To achieve this, a De-Orbit Drag Device (D3) was designed with four retractable measuring-tape-style booms, each 4cm wide (when flat), 3.7 meters long, and inclined at 20 degrees relative to the top face of the satellite. It was shown through simulations that a system in this configuration would be aerodynamically stable up to an altitude of 700 km and would align the z-axis of the satellite (axis going through the drag device) with the velocity vector, providing a predictable attitude profile and maximizing aerodynamic drag. The booms of the drag device could also be differentially deployed such that the resulting gravity gradient torques align a satellite axis perpendicular to the z-axis with the nadir vector. The ability to modulate the spacecraft's drag area by deploying and retracting the booms means that this device could be used for orbital maneuvering and can be used to help the spacecraft target a re-entry point using only aerodynamic forces. Thermal analysis showed that a proper surface finish applied to the booms and boom deployer shells would allow all D3 components to operate within their thermal limits. Additional thermal analysis also showed that the entire system would disintegrate on re-entry and would not create any additional debris.

D3 is the first spacecraft subsystem capable of providing passive 3-axis attitude stabilization while simultaneously modulating the drag area of the spacecraft. This system facilitates drag-based orbital maneuvering and de-orbit point targeting and satisfies the pointing requirement for many small satellite missions. On such missions, use of the D3 would eliminate the need for large, expensive, complex legacy attitude control and thruster systems. After the planned flight demonstration, the D3 will hopefully become a standard tool in orbit and attitude control and debris mitigation for small satellites.

Appendix, Simulation Environment

This appendix details the different reference frames used in this simulation and the means by which the evolution of the state of the spacecraft over time is modeled. The forces and torques acting on the spacecraft are ultimately used to calculate the translational and rotational acceleration of the satellite and determine the position and attitude profile over time using numerical integration techniques.

A. Assumptions and Reference Frames

Several different reference frames are necessary to define the orbital and attitude dynamics of the spacecraft. These are the Earth Centered Inertial (ECI) frame, the orbital frame, the North East Down (NED) frame and the satellite body frame.

The ECI frame is defined with the origin at the center of Earth, $\mathcal{Z}$-axis through the North Pole, $\mathcal{X}$-axis pointing toward the vernal equinox, and $\mathcal{Y}$-axis completing the right handed coordinate system, where $\mathcal{Y} = \mathcal{Z} \times \mathcal{X}$. This frame is not truly inertial since Earth is not fixed in space, but the errors introduced by assuming that it is inertial are negligible for satellites in Low Earth Orbit (LEO). All orbit and attitude propagations must be done with respect to the ECI frame since they are based on Newtonian mechanics, which are only valid in an inertial reference frame.

The orbital frame is defined with its origin on the satellite center of mass such that the z-axis points toward the Earth, the x-axis is perpendicular to the z-axis, lies in the orbital plane, and points in the direction of motion, while the y-axis completes the right handed coordinate system, where $y = z \times x$. In a circular orbit, the x-axis is aligned with the orbit velocity vector.

The NED frame is defined with its origin on the satellite center of mass, the x-axis pointing North, the y-axis pointing East, and the z-axis pointing down. Earth's magnetic field vector at any given point is generally specified in the NED frame.

The origin of the body frame coincides with the satellite center of mass and the axes of the body frame are fixed to the satellite. The orientations of the body frame axes are up to the satellite designer and the vector to every point on the satellite from the body frame origin remains the same regardless of the satellite's orientation. One can envision the body frame as a coordinate axis glued to the spacecraft. Spacecraft attitude is generally specified as an orientation of the body frame

relative to the ECI or orbital frame. Figure 22 provides a schematic of the ECI, orbital, and body reference frames.

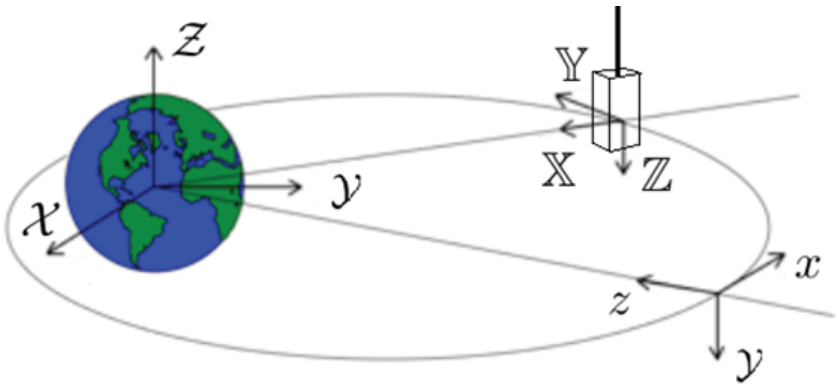

Fig. 22 Schematic of ECI, Orbital, and Body Frames

B. Spatial Rotation

Spatial rotation refers to the method of specifying the orientation of one reference frame relative to another. The ability to do this is crucial for attitude dynamics and control. The primary means of specifying spacial rotations in this work are quaternions and direction cosine matrices.

A direction cosine matrix (DCM) transforms a vector from one reference frame to another. It is a 3x3 matrix that when multiplied by a vector in one frame, gives the representation of that vector in another frame. For example, the ECI to orbital frame DCM can be multiplied by a vector in the ECI frame to provide the representation of the vector in the orbital frame. The transpose of this matrix can be multiplied by a vector in the orbital frame to calculate the representation of that vector in the ECI frame. The direction cosine matrix from reference frame A to frame B (${}^{B}_{A}\mathbf{R}$) can be determined using the basis vectors of frame A represented in frame B as discussed on page 8 of Crane's book [47].

$$ {}^{B}_{A}\mathbf{R} = \begin{bmatrix} {}^{B}\hat{x}_{A} & {}^{B}\hat{y}_{A} & {}^{B}\hat{z}_{A} \end{bmatrix} \tag{34} $$

Since DCMs are orthogonal, the direction cosine matrix from frame B to frame A is given by

$$ {}^{A}_{B}\mathbf{R} = {}^{B}_{A}\mathbf{R}^{T} = \begin{bmatrix} {}^{A}\hat{x}_{B} & {}^{A}\hat{y}_{B} & {}^{A}\hat{z}_{B} \end{bmatrix} \tag{35} $$

To transform a vector $\vec{v}$ from frame A to frame B, the following operation would be performed:

$$ {}^{B}\vec{v} = {}^{B}_{A}\mathbf{R}({}^{A}\vec{v}) \tag{36} $$

If frame B is initially aligned with frame A and rotated by an angle θ about an axis $m = [m_x\ m_y\ m_z]$, then the DCM frame frame B to frame A is given in Eq. 2.61 in Crane's book[47] as

$$ {}^{A}_{B}\mathbf{R} = \begin{bmatrix} m_x m_x v + c & m_x m_y v - m_z s & m_x m_z v + m_y s \\ m_x m_y v + m_z s & m_y m_y v + c & m_y m_z v - m_x s \\ m_x m_z v - m_y s & m_y m_z v + m_x s & m_z m_z v + c \end{bmatrix} \tag{37} $$

where s and c represent the sine and cosine of θ and $v = (1 - \cos(\theta))$. Given a direction cosine matrix of the form

$$ {}^{A}_{B}\mathbf{R} = \begin{bmatrix} r_{11} & r_{12} & r_{13} \\ r_{21} & r_{22} & r_{23} \\ r_{31} & r_{32} & r_{33} \end{bmatrix} \tag{38} $$

the angle of rotation can be calculated by

$$ \theta = \cos^{-1}\left(\frac{r_{11} + r_{22} + r_{33} - 1}{2}\right) \tag{39} $$

The axis of rotation can be calculated by

$$ \begin{bmatrix} m_x \\ m_y \\ m_z \end{bmatrix} = \frac{1}{2\sin(\theta)} \begin{bmatrix} r_{32} - r_{23} \\ r_{13} - r_{31} \\ r_{21} - r_{12} \end{bmatrix} \tag{40} $$

The derivations for Eq. 39 and 40 and a means of calculating the axis of rotation for θ values close to π are given by Crane[47].

Quaternions are another means of representing spatial rotations and are utilized extensively in this study. Quaternions contain one scalar component and three vector components and can be calculated from a given angle (θ) and axis of rotation ($\vec{m}$) using Eq. 12.44 from Crane's book [47] as

$$ q = \cos(\theta/2) + \sin(\theta/2)(m_x\hat{i} + m_y\hat{j} + m_z\hat{k}) \tag{41} $$

It is worth noting that while DCMs were designed to transform a stationary vector into a new reference frame, quaternions were designed to specify the physical rotation of a vector within it's original reference frame. Using quaternions in attitude dynamics can cause some confusion, since vector transformations between reference frames are needed. Some have modified the definition of the quaternion or altered quaternion arithmetic to yield quaternions that transform vectors in a similar manner to DCMs [48]. Different literature sources approach the problem in different ways, so it is important to understand the fundamental assumptions and definitions of the quaternions being used. In this work, the original quaternion definition and set of arithmetic operations given by Hamilton [49] (the creator of quaternions) will be utilized to develop a procedure for vector transformations.

Two important quaternion operations for representing spatial rotations are quaternion multiplication and the quaternion conjugate. Given a quaternion of the form

$$q = d + a\hat{i} + b\hat{j} + c\hat{k} \tag{42}$$

the quaternion conjugate (q^{-1}) is given by

$$q^{-1} = d - (a\hat{i} + b\hat{j} + c\hat{k}) \tag{43}$$

The product of two quaternions of the form in Eq. 42 is given in Eq. 12.13 of Crane's book as

$$q_1 q_2 = d_1 d_2 - a_1 a_2 - b_1 b_2 - c_1 c_2 + d_1(a_2\hat{i} + b_2\hat{j} + c_2\hat{k}) + d_2(a_1\hat{i} + b_1\hat{j} + c_1\hat{k}) \tag{44}$$

To rotate a vector $\vec{r}$ about an axis $\vec{m}$ by an angle θ, a quaternion is first constructed using $\vec{m}$ and θ in Eq. 42. The vector $\vec{r}$ is then represented as a quaternion (r) with zero scalar part. The following operation is then performed to calculate the rotated quaternion-vector r'

$$r' = qrq^{-1} \tag{45}$$

The quaternion r' will also have a zero scalar part and the rotated vector $\vec{r'}$ is simply the vector part of the quaternion. Note that this operation rotates the vector about $\vec{m}$ by an angle θ in the original reference frame. The components of this rotated vector will be the same as the components of the original vector expressed in a reference frame B that is initially aligned with the original

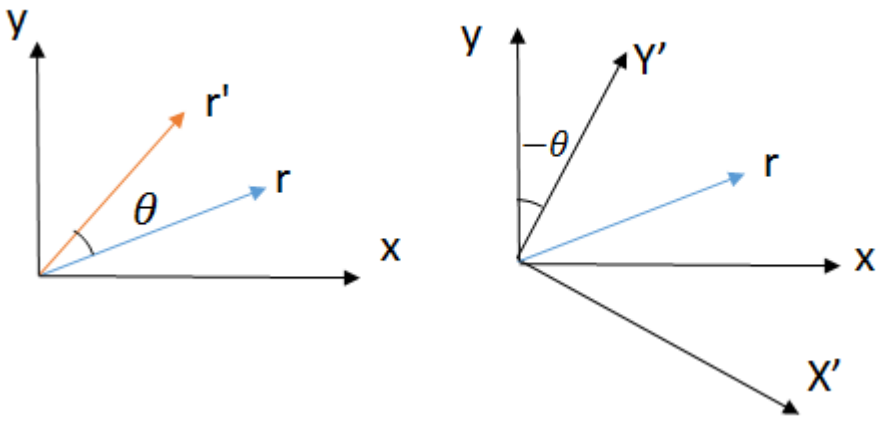

Fig. 23 Rotating a Vector by θ vs. Rotating the Frame by $-\theta$

frame (A) and rotated by an angle $-\theta$ about the axis $\vec{m}$ as illustrated in Figure 23. This important detail is an enormous source of confusion, made worse by the different uses of quaternions. Those in computer graphics and robots are interested in the rotation of vectors within one frame, while attitude dynamicists are concerned with the representation of a given vector in different frames. Fortunately, the solution is simple as long as one keeps careful track of signs and definitions. Given a quaternion represented by an axis and angle of rotation θ, the conjugate of that quaternion is identical to another quaternion representing a rotation about the same axis by an angle $-\theta$. Thus, if frame B is initially aligned with frame A and then rotated by θ about $\vec{m}$ and a quaternion is created using these values of θ and $\vec{m}$, a vector ${}^{A}\vec{r}$ represented in frame A can be converted into a quaternion and represented in frame B as

$$ {}^{B}r = q^{-1}\left({}^{A}r\right)q \tag{46} $$

If a quaternion (q_1) from frame A to frame B and a quaternion (q_2) from frame B to frame C are given, then the quaternion (q_{12}) from frame A to frame C can be calculated by applying the procedure in Eq. 46 twice.

$$ {}^{C}r = q_2^{-1}q_1^{-1}\left({}^{A}r\right)q_1q_2 = q_{12}^{-1}\left({}^{A}r\right)q_{12} \tag{47} $$

$$ q_{12} = q_1q_2 \tag{48} $$

Also important in attitude dynamics is the quaternion derivative. Note that the derivative of a

quaternion relating two reference frames will have a different form than the derivative of a quaternion specifying the orientation within a vector in a single reference frame. Consider frame B rotating with respect to frame A with some angular velocity $\vec{\omega}$ which is constant over an infinitesimally small period of time dt. Let q_0 be a quaternion defining the rotation from frame A to B at some point in time. Since $\vec{\omega}$ is constant over dt, the axis of rotation of B between time t_0 and $t_0 + dt$ is a unit vector ($\hat{n}$) aligned with $\vec{\omega}$ and the the quaternion expressing the rotation of frame B from time t_0 and $t_0 + dt$ is given by

$$q_w = \cos(\theta/2) + \sin(\theta/2)(n_x\hat{i} + n_y\hat{j} + n_z\hat{k}) \tag{49}$$

using the quaternion form of Euler's equation which states that

$$e^{it} = \cos(t) + i\sin(t) \tag{50}$$

q_w can be written as

$$q_w = e^{\frac{\theta}{2}(n_x\hat{i} + n_y\hat{j} + n_z\hat{k})} \tag{51}$$

for a given number t of differential time steps where ω is constant, the total rotation quaternion from frame A to frame B can be calculated as

$$q_{ab} = q_0 q_w^t = q_0 e^{\frac{\theta t}{2}(\hat{n})} \tag{52}$$

Taking the derivative of Eq. 52 with respect to time yields the quaternion derivative

$$\dot{q}_{ab} = q_0 e^{\frac{\theta t}{2}(\hat{n})} \left(\frac{\theta}{2}(\hat{n})\right) \tag{53}$$

Substituting Eq. 52 in Eq. 53 and noting that $\theta\hat{n} = \vec{\omega}$, gives the simplified quaternion derivative equation

$$\dot{q}_{ab} = \frac{1}{2} q_{ab}(\omega) \tag{54}$$

Note that ω in Eq. 54 is a quaternion with a zero scalar part and a vector component equal to the angular velocity of frame B with respect to frame A.

C. Orbital Mechanics

An orbit propagator accurately calculates the spacecraft position and velocity over time which is necessary for orbit lifetime estimation and for calculating the environmental torques needed for the attitude dynamics simulations.

The equation for the acceleration of the spacecraft with respect to the ECI frame is given by the equation [28]

$$\vec{a} = -\mu\vec{r}/r^3 + \vec{F}_{pert}/m \tag{55}$$

where μ is the gravitational parameter of the Earth, m is the mass of the spacecraft, and F_{pert} is the sum of the perturbing forces. Eq. 55 can be integrated to get the changes in spacecraft position and velocity over time. This is done by calling MATLAB's built in ode45 numerical integrator after transforming Eq. 55 to state space form such that the first derivative of each component of the state vector can be written in terms of the current state vector. Note that all orbit propagation is done with respect to the ECI (Earth Centered Inertial) frame and that all vectors must be converted to the ECI frame before Eq. 55 is used.

D. Attitude Dynamics

The attitude of a spacecraft can be defined as the orientation of the spacecraft body frame with respect to some reference frame of known orientation. In this case, attitude will be computed with respect to the ECI frame, since an inertial reference frame is required for Newton's laws to be valid. At any given point in time, there will be a unique axis and angle of rotation ($\hat{n}$ and θ) such that if some frame A, initially aligned with the ECI frame, is rotated about $\hat{n}$ by θ, then frame A will be aligned with the body frame. A quaternion can be formed from $\hat{n}$ and θ using Eq. 49. This is known as the attitude quaternion and always is specified rotating the ECI frame into the body frame. To characterize the evolution of the spacecraft's attitude over time, the angular velocity vector of the body frame with respect to the ECI frame is needed. A 7-element state vector consisting of the four components of the attitude quaternion and the three components of the angular velocity vector are sufficient to completely characterize the attitude dynamics of the spacecraft assuming that the derivatives of this state vector can be calculated. Given the angular velocity and the current attitude

quaternion, the quaternion derivative can be calculated using Eq. 54. The derivative of angular velocity is angular acceleration. The angular acceleration can be calculated based on Euler's second law of motion which states that the summation of external moments (also known as torques) acting on a body is equal to the time rate of change of angular momentum measured about the body's center of mass [50]

$$\sum \vec{M} = \frac{^{E}d}{dt}(^{E}\vec{H}_{cm}) \tag{56}$$

The left superscript E in this equation indicates that the following quantities are computed with respect to an inertial reference frame (the ECI frame in this case). The rate of change transport theorem given on page 47 of Rao's book [50] allows one to compute the rate of change of a vector r in some frame A based on the rate of change of that vector in another frame B and the angular velocity of frame B relative to frame A ($^{A}\omega^{B}$) as

$$\frac{^{A}d}{dt}(\vec{r}) = \frac{^{B}d}{dt}(\vec{r}) + ^{A}\vec{\omega}^{B} \times \vec{r} \tag{57}$$

Applying the transport theorem to compute the rate of change of angular momentum yields

$$\frac{^{E}d}{dt}(^{E}\vec{H}_{cm}) = \frac{^{E}d}{dt}(I_{cm}{}^{E}\vec{\omega}^{B}) = I_{cm}\frac{^{B}d}{dt}(^{E}\vec{\omega}^{B}) + ^{E}\vec{\omega}^{B} \times (I_{cm}{}^{E}\vec{\omega}^{B}) \tag{58}$$

Defining the angular acceleration of the spacecraft body frame with respect to the ECI frame as observed in the body frame as

$$\vec{\alpha} = \frac{^{B}d}{dt}(^{E}\vec{\omega}^{B}) \tag{59}$$

$\vec{\alpha}$ can be calculated as

$$\vec{\alpha} = I_{cm}^{-1}\left(\sum \vec{M} - \vec{\omega} \times (I_{cm}{}^{E}\vec{\omega}^{B})\right) \tag{60}$$

If the initial attitude quaternion, initial angular velocity, summation of external moments, and spacecraft moment of inertia are known, the quaternion derivative and spacecraft angular acceleration can be calculated using Eq. 54 and Eq. 60. These two calculated quantities represent the derivative of the state vector and can be used with a numerical integrator such as MATLAB's ode45 to calculate the evolution of the state vector over time. Combining the 7-element attitude state vector with the 6-element translational state vector yields a 13-element state vector that can

be numerically integrated to provide a 6DOF simulation of the complete dynamics of the spacecraft. For the purposes of this simulation, the initial conditions can be somewhat arbitrarily selected to represent a tumbling spacecraft. The moment of inertia of the spacecraft can also be determined based on the spacecraft CAD model. The remaining challenges in creating an accurate simulator lie in accurately calculating the external forces and torques.

Acknowledgment

The authors would like to acknowledge A.I. Solutions for their help and expertise. This research was funded through NASA Launch Services Program (LSP) subcontract 15-010, and by internal funding from the University of Florida.

References

[1] "Stefan-Boltzmann Constant,".

[2] J. Davis, "Of Inclinations and Azimuths," (2014).

[3] "Nasa Technical Standard NASA-STD-8719.14A," (2012).

[4] D. J. Kessler, N. L. Johnson, J. Liou, and M. Matney, Advances in the Astronautical Sciences **137**, 2010 (2010).

[5] P. Kelly, R. S. Erwin, R. Bevilacqua, and L. Mazal.

[6] R. P. Hoyt, I. M. Barnes, N. R. Voronka, and J. T. Slostad, in *AIAA Space 2009 Conference* (2009) p. 6733.

[7] R. L. Forward, R. P. Hoyt, and C. W. Uphoff, Journal of Spacecraft and Rockets **37**, 187 (2000).

[8] J. Andrews, K. Watry, and K. Brown, in *25th Annual AIAA/USU Conference on Small Satellites* (2011).

[9] K. T. Nock, K. L. Gates, K. M. Aaron, and A. D. McRonald, in *2010 AIAA/AAS Astrodynamic Specialist Conference* (2010).

[10] P. Harkness, M. McRobb, P. LÃijtzkendorf, R. Milligan, A. Feeney, and C. Clark, Advances in Space Research **54**, 82 (2014).

[11] D. C. Maessen, E. D. van Breukelen, B. T. C. Zandbergen, and O. K. Bergsma, .

[12] D. Reintsema, J. Thaeter, A. Rathke, W. Naumann, P. Rank, and J. Sommer, in *Proceedings of the i-SAIRAS* (2010) pp. 244–251.

[13] P. C. E Roberts and P. G. Harkness, Journal of Spacecraft and Rockets **44**, 1195 (2007).

[14] R. P. Patera, K. R. Bohman, M. A. Landa, C. Pao, R. T. Urbano, M. A. Weaver, and D. C. White, in *2nd IAASS Conference Space Safety in a Global World* (2007).

[15] V. Luchinski, R. Murtazin, O. Sytin, and Y. Ulybyshev, Journal of Spacecraft and Rockets **40**, 665 (2003).

[16] R. P. Patera and W. H. Ailor, in *Proceedings of the AAS/AIAA Space Flight Mechanics Meeting* (1998) pp. 9–11.

[17] C. L. Leonard, *Formationkeeping of Spacecraft via Differential Drag*, Master's thesis, Massachusetts Institute of Technology (1986).

[18] T. D. Maclay and C. Tuttle, Advances in the Astronautical Sciences **120**, 763 (2005).

[19] B. Kumar and A. Ng, *Japan Canada Joint Collaboration Satellite âĂŞ Formation Flying (JC2Sat-FF) Mission Design* (2013) Case Study.

[20] D. Pérez and R. Bevilacqua, Journal of Spacecraft and Rockets **53**, 234 (2016 `http://dx.doi.org/10.2514/1.a33332`).

[21] R. Bevilacqua and M. Romano, Journal of Guidance, Control, and Dynamics **31**, 1595 (2008 `http://arc.aiaa.org/doi/10.2514/1.36362`).

[22] R. Bevilacqua, AIAA Journal of Guidance, Control, and Navigation **37**, 1042 (2014 `http://dx.doi.org/10.2514/1.g000008`).

[23] D. Guglielmo and R. Bevilacqua, in *SmallSat Conference* (2014).

[24] "Attitude Determination Control Systems,".

[25] "MAI-400 Specifications,".

[26] "Attitude Determination and Control System,".

[27] M. Lovera, in *2015 American Control Conference (ACC)* (2015) pp. 1867–1872.

[28] D. Vallado, *Fundamentals of Astrodynamics and Applications*, 4th ed. (Microcosm Press, Hawthorne, CA, 2013).

[29] U. S. Atmosphere, *US standard atmosphere* (National Oceanic and Atmospheric Administration, 1976).

[30] J. Picone, A. Hedin, D. P. Drob, and A. Aikin, Journal of Geophysical Research: Space Physics **107** (2002).

[31] K. Omar and M. Briggs, AIAA/USU Conference on Small Satellites (2016).

[32] H. Curtis, *Orbital Mechanics for Engineering Students*, 2nd ed. (Elsevier, 2009).

[33] R. R. Bate, D. D. Mueller, and J. E. White, *Fundamentals of astrodynamics* (Dover Publications, New York, 1971).

[34] "Hysteresis Loop,".

[35] E. ThÃľbault, C. C. Finlay, C. D. Beggan, P. Alken, J. Aubert, O. Barrois, F. Bertrand, T. Bondar, A. Boness, L. Brocco, E. Canet, A. Chambodut, A. Chulliat, P. CoÃŕsson, F. Civet, A. Du, A. Fournier, I. Fratter, N. Gillet, B. Hamilton, M. Hamoudi, G. Hulot, T. Jager, M. Korte, W. Kuang, X. Lalanne, B. Langlais, J.-M. LÃľger, V. Lesur, F. J. Lowes, S. Macmillan, M. Mandea, C. Manoj, S. Maus, N. Olsen, V. Petrov, V. Ridley, M. Rother, T. J. Sabaka, D. Saturnino, R. Schachtschneider, O. Sirol, A. Tangborn, A. Thomson, L. TÃÿffner-Clausen, P. Vigneron, I. Wardinski, and T. Zvereva, Earth, Planets and Space **67** (2015), 10.1186/s40623-015-0228-9.

[36] T. W. Flatley and D. A. Henretty, (1995).

[37] "Magnetic Moment of a Solenoid (Magnetic Moment of a Loop),".

[38] S. Omar, AIAA/USU Conference on Small Satellites (2015).

[39] S. Omar, AIAA Sci-Tech 2017 (2017).

[40] S. R. Omar and J. M. Wersinger (American Institute of Aeronautics and Astronautics, 2014).

[41] R. R. Kumar, D. D. Mazanek, and M. L. Heck, Journal of Spacecraft and Rockets **32**, 806 (1995).

[42] J. Springmann, B. Kempke, J. Cutler, and H. Bahcivan, (2012).

[43] "Intel ® Edison Module," (2014).

[44] "Nasa Space App Challenger Runs Yocto on an Intel Edison-Based Nanosat," (2015).

[45] "Intel Edison Cansat Launched in Black Rock Desert, Nevada," (2014).

[46] J. Wertz, D. Everett, and J. Puschell, *Space Mission Engineering: The New SMAD* (Microcosm Press, Hawthorne, CA, 2011).

[47] C. Crane and J. Duffy, *Kinematic Analysis of Robot Manipulators* (Cambridge University Press, 1998).

[48] J. Diebel, Matrix **58**, 1 (2006).

[49] W. R. Hamilton, The London, Edinburgh, and Dublin Philosophical Magazine and Journal of Science **25**, 10 (1844).

[50] A. Rao, *Dynamics of Particles and Rigid Bodies*, 1st ed. (Cambridge University Press, 2006).